Next Generation Anodes for Lithium-Ion Batteries

First Quarter Progress Report 2019

Jack Vaughey, Point-of-Contact
Argonne National Laboratory
9700 South Cass Avenue
Argonne, IL 60439
Phone: (630) 252-8885
E-mail: vaughey@anl.gov

Brian Cunningham, DOE-EERE-VTO Technology Manager
U.S. Department of Energy, Battery R&D
Phone: (202) 287-5686
E-mail: brian.cunningham@ee.doe.gov

Table of Contents

Silicon Deep Dive Overview

Project Introduction

Silicon has received significant attention as an alternative to the graphitic carbon negative electrodes presently used in a lithium-ion battery due to its high capacity and availability. Compared to graphitic carbons, elemental silicon has nearly an order of magnitude higher capacity (~3600 mAh/g silicon vs 372 mAh/g Graphite), however, several problems have been identified that limit its utility including a large crystallographic expansion (~320%) upon full lithiation, slow lithium diffusion, and high reactivity at high states of charge. Together these physical properties result in particle cracking, particle isolation, electrolyte reactivity, and electrode delamination issues. These chemical reactivity and volume changes are manifested in SEI stability (calendar and life studies) and cycling efficiency issues for the cell. Because of the technological advances possible if a silicon anode can be designed and proven, researchers in multiple disciplines have pushed to understand these physical issues and advance the field and create a viable silicon-based electrode.

Next Generation Anodes for Lithium-Ion Batteries, also referred to as the silicon Deep Dive Program, is a consortium of five National Laboratories assembled to tackle the barriers associated with development of an advanced lithium-ion negative electrode based upon silicon as the active material. This research program has several goals including (1) evaluating promising silicon materials that can be either developed by a team member or obtained in quantities sufficient for electrode preparation by the consortiums facilities, (2) developing a composite silicon-Gr electrode that meets BatPac specifications, and (3) executing full cell development strategies that leverage DOE-EERE-VTO investments in electrode materials and characterization. The primary objective of this program is to understand and eliminate the barriers to implementation of a silicon based anode in a lithium-ion cell. The Five National Laboratories (ANL, NREL, LBNL, ORNL, and SNL) involved are focused on a single program with continuous interaction, clear protocols for analysis, and targets for developing both an understanding and a cell chemistry associated with advance negative electrodes for lithium-ion cells. This undertaking is a full electrode/full cell chemistry project with efforts directed at understanding and developing the chemistry needed for advancing silicon-based anodes operating in full cells. Materials development efforts include active material development, binder synthesis, coatings, safety, and electrolyte additives. Efforts include diagnostic research from all partners, which span a wide range of electrochemical, chemical and structural characterization of the system across length- and time-scales. Specialized characterization techniques developed with DOE-EERE-VTO funding, include neutrons, MAS-NMR, optical, and X-ray techniques being employed to understand operation and failure mechanisms in silicon-based anodes. In addition, several strategies to mitigate lithium loss are being assessed. The project is managed as a single team effort spanning the Labs, with consensus decisions driving research directions and toward development of a functioning stable silicon-based electrode.

The silicon Deep Dive project seeks to identify the limiting factors of silicon-based electrodes that need to be overcome to produce a viable functioning LIB electrode and full cell. The issues include understanding and controlling silicon surface chemistry, lithium loss due to side reactions, active material interactions, and the role of electrolyte stability. The goal of the project is utilize our understanding of silicon and silicide reactivity, electrode formulation, and binder and electrolyte formulations, to design a functioning silicon-based electrode for a lithium-ion cell that meets DOE-EERE goals. Combined with the SEISta's efforts focused on interfacial reactivity, composition, and stability, key variables can be isolated and studied to improve the performance of a silicon-based cell. This key interaction is maintained and accomplished through joint meetings, face to face discussions, and extensive collaborations between the teams.

Current Deep Dive Goals:

Q1   Demonstrate improved cycling efficiency of a silicon-based electrode that incorporates either an inorganic or organic surface modification compared to uncoated silicon baseline

Q2   Exhibit a binder designed to strongly interact with the silicon particle surface that shows enhanced cycling stability versus an LiPAA baseline.

Q3   Demonstrate that controlling lithium inventory in a full cell can extend cycle life of a silicon-based electrode by at least 10%.

Q4   Construct and evaluate cells based on optimizing lithium inventory, binder, electrolyte formulation, and testing protocol to achieve a 300 Wh/kg cell design.

Approach

Oak Ridge National Laboratory (ORNL), National Renewable Energy Laboratory (NREL), Pacific Northwest National Laboratory (PNNL), Lawrence Berkeley National Laboratory (LBNL), and Argonne National Laboratory (ANL) have teamed together to form an integrated program. Technical targets have been developed and regular communications have been established. Throughout the program, there is a planned focus on understanding, insights into, and advancement of, silicon-based materials, electrodes, and cells. All anode advancements will be verified based on life and performance of full cells. Toward that end, baseline silicon-based materials, electrodes, and cells have been adopted, along with full cell testing protocols.
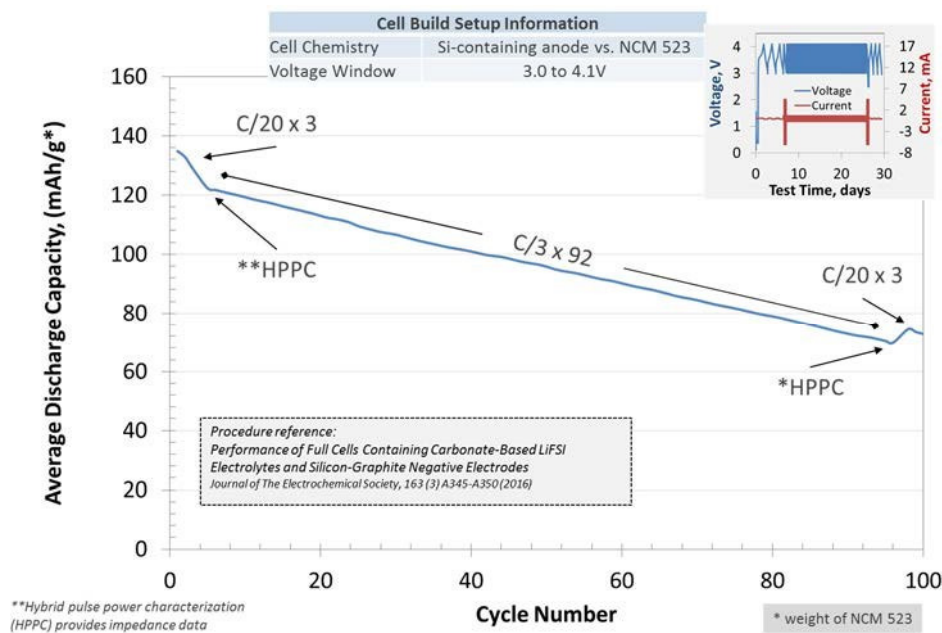
Figure 1. Full cell testing protocol.

In examining improvements, changes to the baseline cell technology will be minimized. As an example, silicon active material coating improvements will be verified on baseline silicon materials in electrodes fabricated by the battery research facilities. All other components in the prototype cells (i.e. positive electrode, separator, and electrolyte) will be from the baseline technology. While there are many testing protocols that can be utilized to benchmark the baseline technology, this program has adopted a testing protocol from the literature

that has worked well for lithium-ion cells with silicon containing anodes. Shown pictorially in Figure 1 the test starts with three slow (C/20) formation cycles, an HPPC cycle, and then the C/3 aging cycles. The test ends with another HPPC cycle and three more slow (C/20) cycles. All constant current cycling is symmetric between charge and discharge rates. The tests are run at 30°C. If there is little or no aging in the first 100 cycles, the protocol can be repeated. This protocol effectively examines capacity, impedance, and aging effects in about a month's worth of testing. As the program matures, materials developments will be incorporated into baseline silicon-based materials, electrodes, and cells. Scale-up of materials, incorporation of materials advancements into electrodes and prototype cells, and characterization and testing of cells, as well as evaluation of safety and abuse tolerance are part of a wide range of integrated studies supported by battery research facilities at the National Labs working closely with the program. These research facilities include the Battery Abuse Testing Laboratory (BATLab), the Battery Manufacturing Facility (BMF), the Cell Analysis, Modeling, and Prototyping (CAMP) facility, the Materials Engineering Research Facility (MERF), and the Post-Test Facility (PTF). At the present time the baseline silicon is from Paraclete Energy (Chelsea, MI).

The fundamental understanding of silicon-based electrode active materials is based on extensive electrochemical and analytical diagnostic studies on components, electrodes, and cells conducted within the program. This effort contains in-situ and ex-situ studies on full and specialty cells, including reference electrode cells. Overall, the diagnostic studies are intended to help establish structure-composition-property relationships, including lithium-reactivity at the silicon surface and bulk transport and kinetic phenomena. Further, they should form the basis for accurately assessing component and electrode failure modes and lay a path for advancements.

Supported by diagnostic studies, materials development on silicon-based materials, electrodes, and cells is being conducted to enhance interfacial stability, accommodate intermetallic volume changes, and improve overall performance and life. Key to this effort is the development and testing of coatings and additives designed to modify and stabilize the dynamic silicon-electrolyte interface. Further, functional polymer binders designed to accommodate volume changes, increase conductivity, and improve adherence are being developed and analyzed. Finally, the program is exploring active material development, including high-energy silicon and silicide materials, development of additional lithium inventory additives, and use of designer passivation materials.

Communication of programmatic progress to battery community is critical. This will generally be accomplished through publications, presentations, reports, and reviews. Further, the program is open to industrial participation and/or collaboration that does not limit program innovation or the free flow of information. Finally, this program is highly integrated with our sister program on SEI-Stabilization (SEISta). In general, SEISta is focused on the development and characterization of model systems, thin-film well-defined active area electrodes on which it is easier to extract fundamental information on lithium-silicon phase formation, lithium transport, and interfacial phenomena (e.g. SEI formation and growth).

Milestone FY2019Q1

Demonstrate improved cycling efficiency of a silicon-based electrode that incorporates either an inorganic or organic surface modification compared to uncoated silicon baseline

Within the DeepDive Silicon effort, there are three groups focused on addressing the role of coatings and cycling of a silicon based electrode. Two PIs (Gao Liu (LBNL), Dan Abraham (ANL)) have been studying the role of carbon coatings and John Zhang (ANL) has been evaluating silicon surfaces functionalized with either hydrophobic or hydrophilic groups.

Dan Abraham has been seeking to alter the silicon particle surfaces through evaluation of several coated silicon materials. Samples used were the Paraclete baseline (C-coated silicon) and, for comparison, the previous NanoAmor baseline (uncoated silicon). Previous work by ANL - CAMP and ORNL (Veith, Ruther) had shown that carbon coated silicon particles had lower catalytic activity than uncoated silicon surface as reflected by reduced hydrogen generation during the preparation of electrode slurries based on silicon oxidation by water.

$$Si + 2H_2O \rightarrow SiO_2 + 2 H_2\uparrow$$
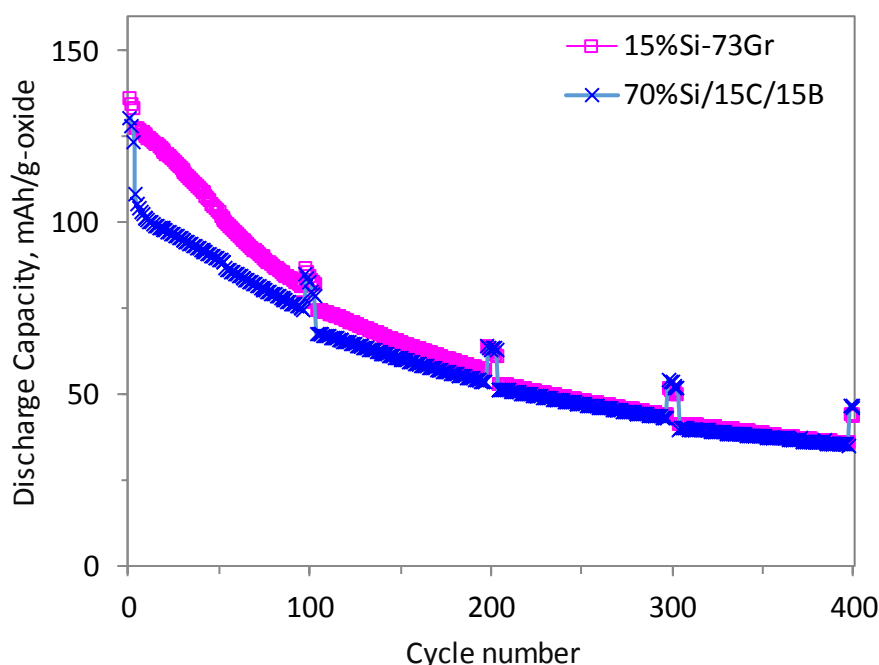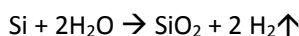
Additionally, full cells containing the carbon-coated silicon particles display higher initial capacity, and greater capacity retention, than cells containing non-coated silicon particles.

Figure 2. Discharge capacity vs. cycle number for an NCM523/15Si cell (magenta plot) and an NCM523/70Si cell (blue plot) tested at 30°C. The test protocol contained four repetitions of 100 cycles. In each of these 100 cycles, cycles 1-3 are at a ~C/20 rate, 4-97 are at a ~C/3 rate and 98-100 are at a C/20 rate.

In this quarterly report, the Abraham group compared the cycle life of a 15% carbon-coated Si electrode to a 70% carbon-coated Si electrode. The key observation was that the difference in first cycle Coulombic efficiency values resulted from a greater loss of Li$^+$ ions to the SEI in the 70Si cell during the first charge cycle. The capacities continue to decrease during the early cycles with continued SEI formation; however with cycling, the CE increases with cycle number indicating progressively decreasing Li$^+$ loss to the SEI. Figure 2 shows that the capacity differences between the 15Si and 70Si cells decrease with cycling. The 15Si cell loses capacity at a faster rate, especially during the 1st 100 cycles, compared to the 70Si cell. The faster capacity loss results from a greater volume changes in the silicon particles during lithiation/delithiation of the 15Si electrode as its cycling profile involves complete lithiation of the silicon. These greater volume changes continuously expose new surface area for SEI formation leading to a faster Li$^+$ loss. Thus at cycle 100 (C/20 rate), the charge and discharge capacities for the 15Si cell and the 70Si cell are nearly equal with regard to the capacity of the 532NMC cathode used. After cycle 200, the slope of the capacities for both cells overlap indicating that the capacity loss is determined by the amount of capacity transferred during the cycling, rather than the silicon content of the electrode. Even after 400 cycles, the cells contain cycleable Li$^+$ ions. In previous reports we studied the baseline uncoated 50-70 nm NanoAmor silicon and consistently noted negligible cycleable Li after only 200 cycles.

While the previous surface catalysis studies focused on an amorphous carbon coating, Gao Liu (LBNL) has initiated a study on the role of the crystallinity of the carbon coatings and shown that the more crystalline the carbon the more stable the endmember phase, Li$_{3.75}$Si, and the higher the observed capacity for the initial cycling. In each case a high temperature process was used to create the carbon coating from an organic precursor on the surface of the silicon nanoparticles. Different precursors were used to form two different carbon coatings; one is a dense highly graphitized coating derived from a polymer precursor and other a disordered carbon structures derived from sucrose. In his study the silicon with the graphitized coating led to formation of the lithiated endmember phase and delivered higher gravimetric capacity and more stable cycling when compared to the silicon coated with disordered carbon coating, where the lithiated endmember phase did not emerge as a major component within the amorphous silicon matrix.

In contrast to the use of inorganic carbon coatings, the Zhang group at Argonne has been evaluating the utility of surface bonded functional groups to create an artificial SEI and help reduce the active lithium loss during the SEI formation process. For these materials, the cycling performance of the cell was shown Figure 3. (a)
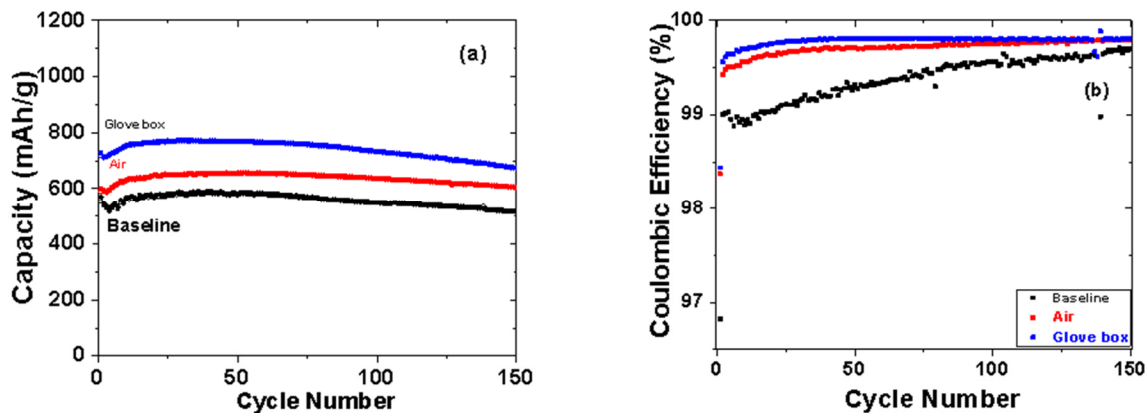
Capacity retention (lithiation: solid; delithiation: empty) and (b) the Coulombic efficiency of silicon-graphite/Li cells.

in Figure 3 with various oxide-containing sidechains. Baseline uncoated silicon-graphite anodes have an initial (delithiation) capacity of 552 mAh/g. The early cycling decreased capacity issues (see Figure) might be due to the electrolyte wetting issue. The initial capacity of the anode containing silicon-C3-EO-Epoxy is much higher (717 mAh/g) with a higher capacity retention (94.1%). However, for the anode containing silicon-C3-EO-Epoxy handled in air, also had an initial capacity increase compared to baseline (590 mAh/g) but with the best capacity retention (95.1%) among all studied materials. In terms of Coulombic efficiency, the pristine Si NPs showed the first cycle Coulombic efficiency of 96.8%, the surface functionalized in the presence of air samples yielded a 98% efficiency and the glovebox prepared and functionalized Si NPs electrodes stabilized at 99.7%. This result clearly indicates the surface functional groups could sufficiently suppress the side reactions of the Si NPs preventing the active lithium loss at the anode/electrolyte interface.

Summary: In Q1, the effort has indicated that the surface of the silicon nanoparticles can have a significant effect on the electrochemistry and that the type of coating has strong implications on performance. The carbon coating efforts have shown that the crystallinity of the carbon impacts the formation of the crystalline $Li_{3.75}Si$ endmember phase, with a more graphitized carbon favoring its formation over an amorphous coating. Additionally it was also demonstrated that the amorphous carbon phases presently coated on our baseline samples by the manufacturer play a significant role in capacity retention and extension of cycle life, regardless of the percent of silicon in the electrode when compared to previous uncoated commercial silicon samples. These observations build on our observation that uncoated silicon results in more gassing and hydrogen release during slurry preparation. Additional efforts to suppress lithium loss to side reactions using organic surface functionalization have been successful as the epoxy-derived surface bonded coating appears to suppress side reactions possibly by limiting the diffusion of solvent molecules to the active lithiated surface, limiting the loss of active lithium. This translates to a near 3% increase in Coulombic efficiency.

Silicon Baseline Evaluation

At our September 2018 meeting, we were asked to evaluate and catalogue the number of silicon materials being used in the DeepDive program and to eliminate ones being used by fewer program participants. At that time 11 different silicon's were being used across the DeepDive effort. After the meeting we encouraged researchers to use the carbon coated Si (from Paraclete Energy) baseline. Several researchers with long term cycling studies are still using the previous NanoAmor baseline but intend to transition when appropriate. The next generation Paraclete (scaled up) baseline was still under study by CAMP and has not yet been distributed. The ORNL team continues development of a coated ground silicon that would be under DOE control. The NREL team continues to improve on methods to scale up a silicon material with a hydride passivation layer, which is particularly important to the surface functionalization teams. Overall we have two primary silicon's being used, three under evaluation, and eliminated the use of 7 silicon materials and are close to eliminating one more as of this quarter.

Composite Silicon / Graphite Electrodes

Variable Temperature Performance of Silicon-Gr Composite Electrodes

María José Piernas, Ira Bloom, Alison Dunlop, S. Trask, A. Jansen

Background

Silicon is considered as a promising anode material to replace graphite in Li-ion batteries for electric vehicle (EV) applications, given the high capacity and, hence, the high energy density of this material. However, one factor that hugely affects the battery performance and that should not be overlooked, especially considering its ultimate goal, is the temperature at which an EV operates. To the best of our knowledge, the effect that temperature has in the cyclability of silicon has not been reported so far. In this project, we explore the effect of temperature on the electrochemical performance of silicon anodes.

Results

We plan to study four different material/electrolyte systems in this effort: silicon in Gen 2 (1.2 $\underline{M}$ LiPF$_6$ in EC:EMC, 3:7 by wt) electrolyte, silicon in Gen 2 electrolyte + 10 wt% fluoroethylene carbonate (FEC), silicon/graphite (silicon/Gr) in Gen 2, and silicon/graphite in Gen 2 electrolyte + 10 wt% FEC. In this report, we will discuss the data obtained from the silicon/graphite cycled in Gen 2 electrolyte only. siliconnce silicon is known to display continuous lithium consumption and SEI (solid electrolyte interphase) formation during the cycling process, metallic lithium is used as a counter electrode in our study to eliminate the possibility of lithium depletion.
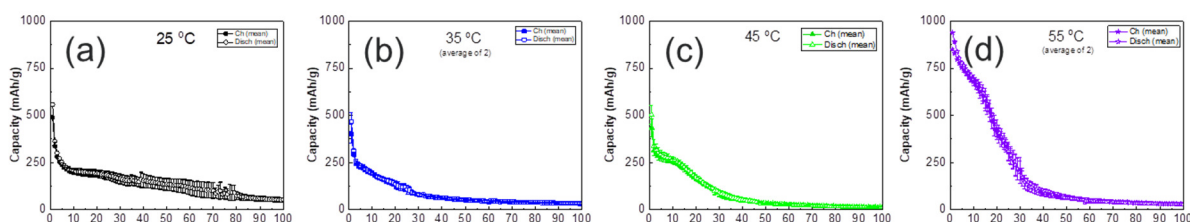
Figure 4. Charge and discharge capacity *versus* cycle number plot of silicon/Gr half-cells containing Gen 2 electrolyte and cycled at (a) 25, (b) 35, (c) 45 and (d) 55 ˚C. The filled and empty markers represent, respectively, the charge and discharge capacities. In all the cases the silicon/Gr electrode was from CAMP (A-A013).

Figure 4 displays how the capacity of a silicon/graphite (silicon/Gr) electrode varies as a function of cycle count and temperature applied. After the initial capacity drop during the first 3 cycles at all temperatures (a result of the SEI formation), the rate of capacity fade changed with time at temperature, being more gradual at 25 ˚C (Fig. 4a) and more abrupt when the temperature is increased (Fig. 4b, c and d). At temperatures greater or equal to 35˚C, all capacity was lost after 30 cycles. Another interesting observation was that the discharge capacity also differed with the temperature (**Fig. 5a**). In the 5th cycle, the discharge capacity was ~200 mAh/g at 25 and 35˚C;
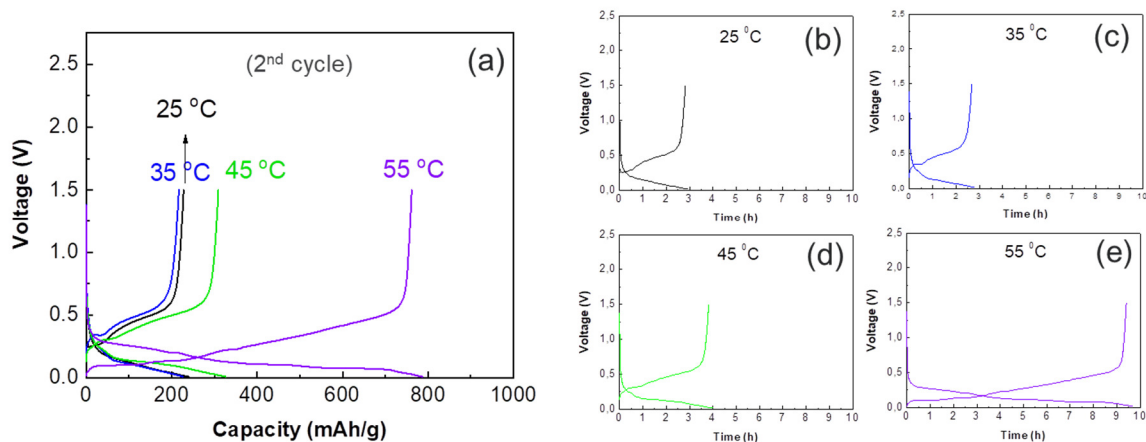
Figure 5. (a) Voltage versus capacity for the second cycle (after the three first formation cycles) of silicon/Gr half-cells and their corresponding voltage versus time plots at (b) 25, (c) 35, (d) 45 and (e) 55°C. In all the cases the silicon-graphite electrode was from CAMP (A-A013).

~300 mAh/g at 45°C; and almost 800 mAh/g at 55°C. In all cases, the same current being applied (ca. 350 µA). Larger capacities were observed the higher the temperatures, probably due to a better Li$^+$ diffusion leading to a lower effective C-rate, as shown in **Figs. 5b**, **c**, **d** and **e**. Note that the time necessary to complete the charge subcycle was ~3h at 25 and 35°C; ~4h at 45°C; and ~10 h at 55°C. It is also possible that the higher temperature lead to a more stable SEI layer, leading to less disintegration of silicon.

Conclusions

Some results of silicon/Gr half-cells cycled in Gen 2 electrolyte at several temperatures were discussed. We find that temperature influenced the capacity obtained and, thereby, the effective C-rate. The higher the cycling temperature, the larger the capacity achieved and the lower the C-rate. However, the capacity fade varied with temperature and capacity fade was faster at higher temperature. We think that the fading mechanism changed with temperature, which we will study in the near future.

Silicon – Containing Anodes with Extended Cycle Life and Calendar Life

Ji-Guang Zhang, Xiaolin Li (PNNL)

Nanoscale silicon, a highly porous structured silicon material, has been widely used as a stable silicon electrode component in an effort to avoid pulverization of silicon particles during cycling process. However, the large surface area of nanosilicon or micron sized porous silicon also has been noted to lead to a continuous reaction between lithiated silicon and electrolyte, with evidence of gassing or electrode degradation reported. As a result of these reactions, continuous growth of SEI layer and increase of cell impedance have been noted. Another possible degradation mechanism is cross-talk within the cell between silicon anode and cathode. This event, for example dissolution of Mn from the surface of an NMC or spinel cathode followed by cation transport to the anode side, can poison the anode SEI. The addition of FEC as an additive has been shown to form an effective and stable SEI layer on silicon but may also form a electrolyte-based film at the cathode interface (CEI) leading to an impedance increase. Our goal is to minimize the surface area of silicon and find a stable electrolyte additive are critical for long term stability of silicon based Li-ion batteries.

In this project, we seek to enhance the cycle life and calendar life of silicon-based Li-ion batteries by creating a stable porous silicon structure in conjunction with an artificial SEI layer coating. In association with these objectives, a more stable electrolyte additive or solvent mixture will be investigated to minimize the effect of FEC at the cathode interface. The degradation mechanism of silicon anodes during shelf storage will be systematically investigated. New insights on these mechanisms and the new approaches developed in this work will speed up the deployment of high energy Li-ion battery with silicon-based anodes and increase market penetration of EVs and PHEVs as required by DOE/EERE.

Results

In this quarter, stability of silicon anodes have been further investigated in (LHCEs) developed in PNNL using silicon/Gr anodes and NMC532 cathode obtained from CAMP facility. As shown in Table 1, several electrolytes with different salt concentrations were investigated. The results of electrochemical tests shown in Figure 6a and Table 1 indicate that the LHCEs consist of BTFE diluted LiFSI-EC:EMC can greatly improve the cycling stability and first Coulombic efficiency (FCE) of full cells. Electrolyte E-104 (1.8M LiFSI in EC-EMC (3:7 by wt.)-2BTFE (molar ratio to EC/EMC) + 5 wt% FEC) enables the best overall performance of the cells considering the specific capacity (114.8 vs 96.3 mAh/g for 4th cycle), FCE (75 vs 60%) and cycling stability (92.4 vs 55% over 100 cycles) comparing to the baseline electrolyte (1.2 M LiPF6 in EC-EMC (3:7 by wt.) +10 wt.% FEC).

The study also revealed that further increase or decrease of BTFE diluent concentration in LHCEs leads to degraded performance parameters. In another effort, the effect of carbon coating on silicon active material was also investigated to study the surface chemistry effect on battery performance. The silicon nanoparticles (Paraclete Energy) were coated with carbon via a CVD method using acetylene as the carbon source. The CVD process was carried out at 700 C for 30 min under a mixture of argon and acetylene gas. The amount of carbon coating is calculated to be 10 wt%. Polyimide (PI) binder was introduced to further improve the electrode integrity. Although PI binder leads to lower specific capacity when the baseline

Design of experiments summary table				
	Electrolyte	FCE	Specific capacity@4th cycle (mAh/g)	Retention @ 100th cycle
Baseline	1.2 M LiPF$_6$ in EC-EMC (3:7 by wt.) +10 wt.% FEC	60%	96.3	55%
E101	6M LiFSI in EC-EMC (3:7 by wt.) + 5 wt% FEC	60%	41.8	40%
E102	2.9 M LiFSI in EC-EMC (3:7 by wt.)-1BTFE (molar ratio to EC/EMC) + 5 wt% FEC	73%	99.1	71%
E103	2.5 M LiFSI in EC-EMC (3:7 by wt.)-1.5BTFE (molar ratio to EC/EMC) + 5 wt% FEC	75%	117.6	67%
E104	1.8M LiFSI in EC-EMC (3:7 by wt.)-2BTFE (molar ratio to EC/EMC) + 5 wt% FEC	75%	114.8	95%
E-105	1.2M LiFSI in EC-EMC (3:7 by wt.)-3BTFE (molar ratio to EC/EMC) + 5 wt% FEC	70%	82.9	71%

Table 1. Electrochemical performance of NMC532‖silicon/Gr (CAMP electrodes) full cell in BTFE-based electrolytes with different salt concentration.
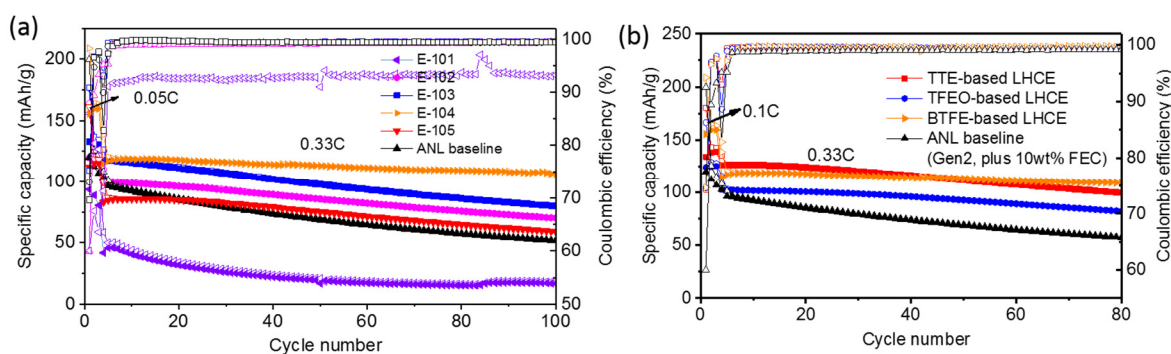
Figure 6. a) Cycling performance of NMC532‖silicon/Gr (CAMP electrodes) in BTFE-based electrolytes with different salt concentration; b) cycling performance of NMC532‖ silicon/Gr (CAMP electrodes) in BTFE, TTE and BTFE-based electrolytes.

electrolyte (Gen2, plus 10 wt% FEC) is used as shown in Table 2, the use of LiFSI-TEPa based LHCE instead of baseline electrolyte can largely improve the cycling stability of the modified silicon anodes. 1.2 wt% of FEC additive was added in E313 electrolyte to further improve the cyclability of NMC532‖silicon/Gr cells. For the full cell test, silicon anodes were pre-lithiated using Li metal in half cells (3 formation cycles) due to the higher initial irreversible capacity from PI binder. The results in Table 2 show that the full cell with LiFSI-TEPa-FEC based LHCE demonstrated better cycling stability and slightly higher capacity. In the next quarter, fundamental mechanism behind these improved electrochemical performances will be further investigated through in-depth collaboration with the teams in the silicon consortium.

Anodes	Prelithia-tion	Electrolyte		FCE	Specific capacity @ 4th cycle	Retention @ 100th cycle
Deep dive anode silicon-PAALi	No	Baseline	1.2M LiPF6 in EC/EMC-10% FEC	60%	96.3	53.4%
PI-carbon coated silicon	No	E-313	1.2M LiFSI/TEPa-3BTFE (molar ratio to TEPa)	55%	78	86.5%
	Yes	E-313		78%	92.8	90.3%
	Yes	E-313+FEC	1.2M LiFSI/(TEPa:FEC)-3BTFE (molar ratio to TEPa)	76%	92.3	95%

Table 2. Representative values for the first cycle efficiency, specific capacity and capacity retention (100th cycle) of NMC532‖ silicon/Gr (modified electrodes) full cell in LiFSI-TEPa based LHCEs.

Conclusions

Localized high concentration electrolytes using BFTE diluents can greatly improve the cycling stability and first Coulombic efficiency (FCE) of silicon based anodes with LiPAA binder. NMC532||silicon/Gr (CAMP electrodes) cells using LHCE of 1.8 M LiFSI in EC-EMC (3:7 by wt.)-2BTFE + 5 wt% FEC exhibits the best electrochemical performance (~114.8 vs. 96.3 mAh/g after formation cycle) and cycling stability (92.4% vs. 60% over 100 cycles).

Impact of Processing Conditions on Uniformity of Silicon-Gr Composite Electrodes (ORNL)

Rose E. Ruther, Beth L. Armstrong, Jagjit Nanda, and Gabriel M. Veith (ORNL)

Background

Prior work on silicon-Gr composite electrodes showed that it can be challenging to process uniform composite electrodes with a homogeneous distribution of silicon throughout.[1] Conventional processing yields electrodes that segregate into graphite-rich and silicon-rich regions with large agglomerates of silicon and carbon black. Achieving a homogenous electrode is important to improve electronic conductivity, accommodate silicon volume expansion, and prolong cycle life. Electrode uniformity can be improved by introducing dispersants during slurry processing. In this work, Raman spectroscopy and mapping were used to evaluate the distribution of silicon in silicon-Gr composite electrodes prepared using different combinations of dispersants and binders. Raman spectroscopy is well-suited to study silicon-Gr composites because silicon, graphite, and carbon black are all strong Raman scatterers with unique vibrational signatures.

Results
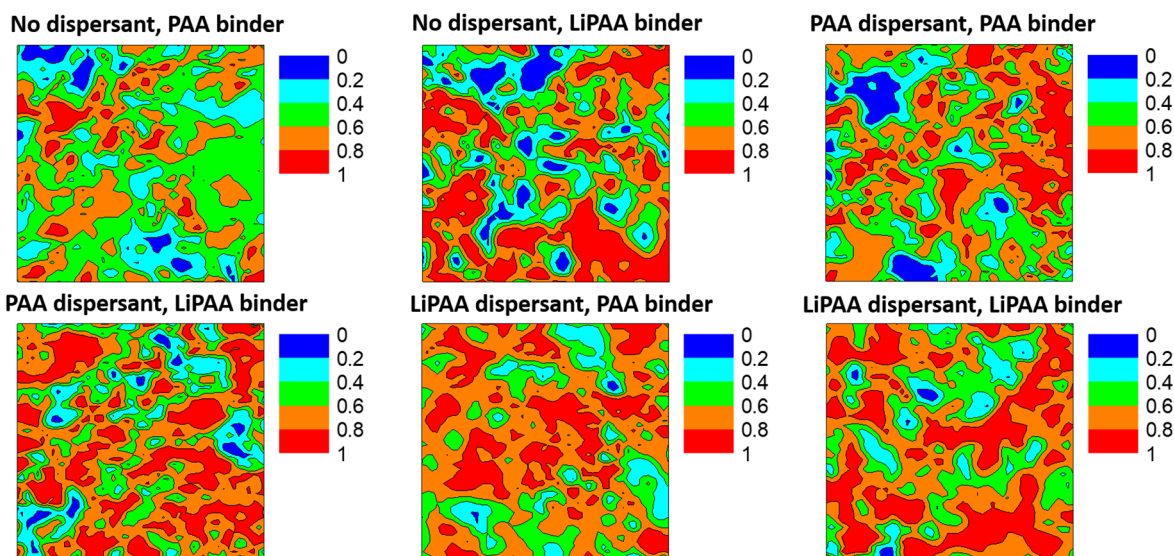
Figure 7. Raman maps of the relative fraction of silicon across electrodes processed using different dispersants and binders. Each map is 50 μm x 50 μm and represents 2500 spectra collected at 1 μm^2 resolution. The most uniform distribution of silicon is obtained when LiPAA is used as a dispersant.

silicon-Gr anodes processed from six different slurries were compared. The slurries used either no dispersant, polyacrylic acid (PAA) dispersant, or lithium polyacrylate (LiPAA) dispersant. Two different binders, PAA and LiPAA, were also compared. Raman maps of the relative fraction of silicon across each electrode are shown in Figure 7. While all anodes have regions that are relatively silicon-rich (red) and silicon-poor (blue), the processing conditions have a clear impact on electrode uniformity. Silicon-Gr composite anodes that were processed using LiPAA as a dispersant have the most homogeneous coating of silicon across the electrode area. These electrodes have relatively fewer regions with little or no silicon shown in blue. This was true independent of whether LiPAA or PAA was used as the electrode binder.

Conclusions

Using LiPAA as a dispersant during slurry processing greatly improved the uniformity of silicon-Gr composite anodes. LiPAA was more effective than PAA as a dispersant. The choice of binder (LiPAA or PAA) did not have an obvious impact on electrode uniformity. These results show that careful control of processing conditions can improve the quality of electrode coatings, which is expected to lead to enhancements in rate capability and cycle life.

References

1. Ruther, R. E.; Hays, K. A.; An, S. J.; Li, J.; Wood, D. L.; Nanda, J., Chemical Evolution in Silicon–Graphite Composite Anodes Investigated by Vibrational Spectroscopy. ACS Appl. Mater. Interfaces 2018, 10 (22), 18641-18649

Binders and Surfaces for Composite Silicon/Gr Electrodes

Bi Hu, Sisi Jiang, Jingjing Zhang, Zhengcheng Zhang, Lu Zhang (Argonne National Laboratory)

Background

In this project, we have been working on understanding and re-engineering the crucial supporting materials for silicon lithium-ion batteries. Some efforts include understanding the property/cycling relationship of PAA binders, and re-engineering PAA based binders. In this quarter, several items will be discussed including PAA-based slurry stabilization and silicon stability and the re-engineered poly (4-vinylbenzoic acid) or P4VBA binders have been evaluated in full cells and the cycled electrodes were analyzed.

Results

Pre-lithiation of PAA binders: A new set of full cells have been fabricated with more reasonable NP ratios (ranging from 1.1 to 1.4) and a CAMP supplied cathode, $LiNi_{0.5}Co_{0.2}Mn_{0.3}O_2$ (NCM523, C-013A), was used to couple with silicon-Gr composite anodes. The full cells were subjected to a standard testing protocol, containing three formation cycles at a nominal C/20 rate, a hybrid pulse power characterization (HPPC) test, ninety-two aging cycles at a C/3 rate, another HPPC test and three final cycles at a C/20 rate, for a total of 100 cycles with the cell voltage between 3.0-4.2 V. The specific capacity profiles are shown in **Figure 81**. The controlled NP ratios indeed afford a different view of full cell cycling. From **Figure 8**, the observed trend based on the average capacity is **PAA-2.1>PAA-4.2>PAA-6.0>PAA-4.8>PAA-7.0**, which is more consistent with the half-cell cycling results. Peeling test was used to assess the adhesive/cohesive strength of the electrode. As shown in **Figure 8c**, the load profiles indicate that the increased lithiation of PAA decreases the cohesion in the matrix. This can be attributed to the reduced number of COOH groups that can esterify Si-OH groups at the surface of silicon particles, forming strong bonds between the polymer chains and the silicon particles. Overall, this study indicates that less pre-lithiation seems more beneficial to silicon-Gr composite anodes.
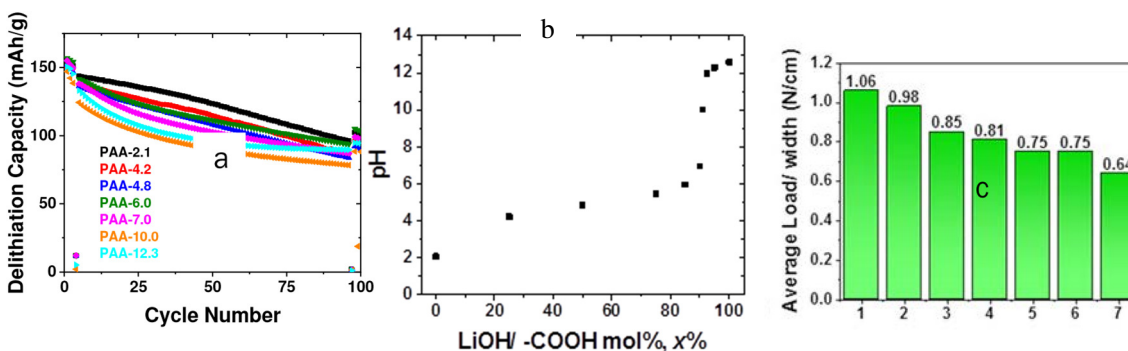
Figure 8. (a) Specific dilithiation capacity profiles for NCM523/silicon-Gr full cells containing lithiated PAA binders with different pH values. (b) Equivalence curve for the lithiation of the PAA Binder. (c) Average load/width with a range of 50 mm for silicon-Gr electrodes. Numbers correspond to the pH samples (1= lowest (pH= 2.1), 7 = highest (pH = 12.3)).

Engineering PAA-Poly (4-vinylbenzoic acid) (P4VBA) binders: conjugated P4VBA-based binders have shown improved cycling performance of silicon-Gr half cells using NMP solvents during lamination. These P4VBA-PAA binders, constructed using Reversible Addition Fragmentation Chain Transfer (RAFT) showed improved elasticity properties and better viscosity when compared to the PAA-baseline. In collaboration with other team members we have been evaluating the surface functionality as our system binds through surface

silanols (Si-OH) and how these new binders (See **Figure 9**) interact with the surface of the Paraclete silicon baselines. Preliminary data indicates that some modifications are needed to optimize the interactions.
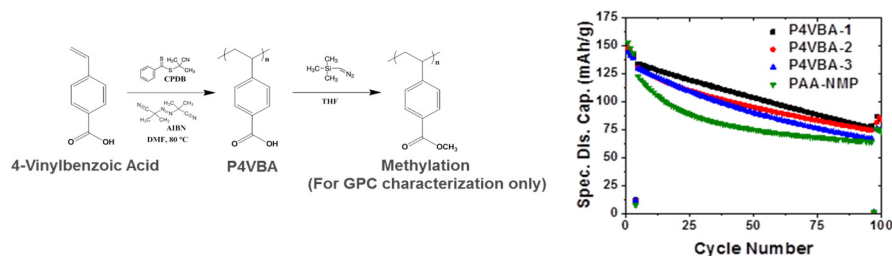
Figure 9. Synthesis route for the P4VBA-based binders and their cycling stability with an NMC 532 cathode

Conclusions

This quarter we continue to work on binders for silicon-Gr composite electrodes. Full cell tests using Lix[PAA] binders have been redone and the new results are consistent with the half-cell. We tested PAA-P4VBA binders, a family of re-engineered PAA based binders, in full cells and evaluated them in full cells. Prelimiary data indicates that although they have good properties, some optimization of the functional groups (Paraclete silicon) would be beneficial to performance.

The Role of Dispersants on Binder Selection for silicon-Gr Composite Electrodes (ORNL)

Beth L. Armstrong, Kevin Hays, Rose E. Ruther, and Gabriel M. Veith (ORNL)

Background

Selection of a binder designed to strongly interact with the silicon particle surface that shows enhanced cycling stability versus the LiPAA baseline system has been a challenging task. Prior work on silicon-Gr composite electrodes did not yield homogeneous distribution of silicon throughout the electrode structure.[1] The dispersion of the silicon, graphite and carbon black prior to the down-selection of a binder system is critical to achieving a homogenous electrode to improve cycle life and stability. In the previous work, the binder was carrying the role of both dispersant and rheology modifier/processing aid. The role of the dispersant was separated from the binder to determine if electrode homogeneity could be improved. Rheology was used to characterize the silicon-Gr-carbon black (CB) composite slurries to study the relationship between the dispersant, binder and cycle performance.

Results

Binders typically have several functions in the fabrication of a battery electrode. The primary function is to create cohesion between particles, between particles and the current collector, and to provide strength during processing, handling and use. Although a binder can contribute to the suspension of powders in the solvent, the binder's molecular weight is typically too long to be an optimum dispersion mechanism.   To maintain compatibility to the existing CAMP formulation, polyacrylic acid (PAA) and lithium polyacrylate (LiPAA) dispersants utilizing molecular weights (~1.2K) sized appropriately to the particle size of the constituents were evaluated with PAA and LiPAA binders of the higher molecular weights used previously (~240K). The rheological behavior of six silicon-Gr-CB anode slurries were compared as a function of varying dispersant and binder compositions as shown in Figure 10. The slurries used either no dispersant, PAA dispersant, or LiPAA dispersant, and the two different binders, PAA and LiPAA. Both the PAA and LiPAA binder exhibited shear thinning behavior through most the shear range between 1 and 1000 s^{-1}, although the PAA binder shear thickened at shear rates greater than 1000 s^{-1}. The slurries processed with the PAA binder had lower viscosity values as compared the LiPAA binder slurries irrespective of which dispersant was utilized or not.
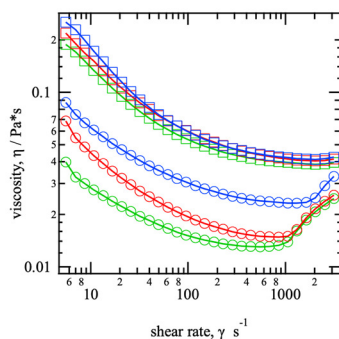
Figure 10. Rheological characterization of silicon-Gr-CB anode slurries: LiPAA dispersant– Blue, PAA dispersant – Red, No dispersant – Green. Circles – PAA binder, Squares – LiPAA binder added.

The effectiveness of the dispersion is further described by the average particle sizes of the particles in the slurry measured by dynamic light scattering, Figure 11. The most benefit for reducing particle agglomeration and improving dispersion is realized by the LiPAA dispersant with either binder system used. No dispersant yields the largest agglomerates, but the PAA dispersant produces similar sizes (> 300 nm).   Overall, the average agglomerate sizes are small in spite of the large micron sized starting graphite particle sizes. Either the graphite is settling out during the measurement and/or the combination of improved order of addition during processing or the use of a dispersant is showing effective reduction in particle agglomeration during the slurry process.
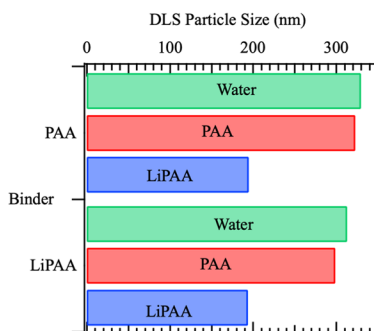
Figure 11. Particle siliconzes of silicon-Gr-CB anode slurries measured using Dynamic Light Scattering (DLS)

The effect of the role of the dispersant is further reflected in the cycling data as shown in Figure 12. The LiPAA dispersant mixed with the PAA binder achieves the best rate performance, and the PAA binders have better rate performance than the LiPAA binder system in spite of the low 1st cycle coulombic efficiency of the PAA binder with the PAA dispersant. The reduced particle sizes of the LiPAA dispersant-based slurries as well as the more uniform distribution of the silicon-Gr-CB particles in the electrode result in improved electrochemical stability.
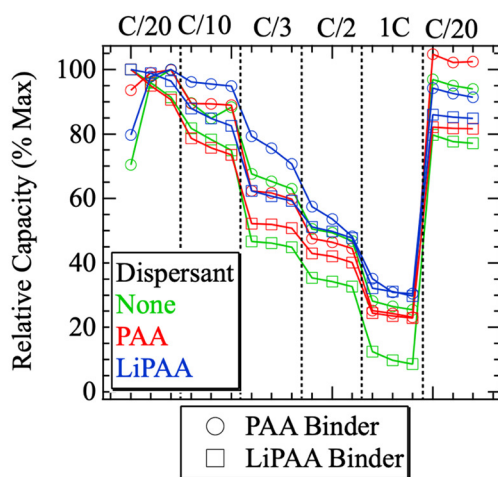
Figure 12. The effect of dispersant is further reflected in the cycling data

Conclusions

Using LiPAA as a dispersant during slurry processing greatly improved the size distribution of silicon-Gr-CB in the composite anodes. In this study, the LiPAA was more effective than PAA as a dispersant. The choice of binder (LiPAA or PAA) did not have an obvious impact on electrode uniformity, although impacted the viscosity and flow behavior of the slurries at high shear rates. These results show that utilizing a separate dispersant may allow for continued use of existing binders while improving the quality of electrode coatings, which is expected to lead to enhancements in rate capability and cycle life.

References

1. Ruther, R. E.; Hays, K. A.; An, S. J.; Li, J.; Wood, D. L.; Nanda, J., Chemical Evolution in Silicon–Graphite Composite Anodes Investigated by Vibrational Spectroscopy. ACS Appl. Mater. Interfaces 2018, 10 (22), 18641-18649

Next Generation Anodes for Lithium-Ion Batteries (LBNL)

Wei Tong (LBNL)

Background

In FY18, we successfully synthesized amorphous silicon (a-silicon) thin films free of binders and conductive carbon additives on Cu current collectors by direct current (DC) magnetron sputtering. silicon-Sn thin film was then prepared by the optimal condition identified from silicon film study using a single silicon-Sn target. In FY19, we direct our tasks to address two aspects in thin film production; (1) change of Cu foil substrate regarding surface roughness (roughened vs. smooth surface for previous and new Cu foils, respectively) and (2) use of new sputtering instrument enabling co-sputtering of multiple targets. The ultimate goal of such developmental work is to identify promising silicon-based thin film compositions as model electrodes for interfacial studies as well as providing guidance for synthesis of silicon-based thin splats by splat quenching method. In FY19 Q1, we first verified the use of new Cu foil substrate with smooth surface for silicon-Sn thin films. Afterwards, we explored the synthesis of individual silicon and Sn films on new Cu foil substrate using new sputtering instrument in order to identify the optimal process parameters for co-sputtering. Physical and electrochemical properties of the as-produced films were investigated using X-ray diffraction (XRD), scanning electron microscopy (SEM), energy-dispersive X-ray spectroscopy (EDS), and electrochemical methods.

Results

Si-Sn film was directly deposited on a new Cu foil with smooth surface (12 μm thickness) by DC magnetron sputtering using the same conditions reported previously. Such silicon-Sn thin film deposition was performed on single silicon-Sn target of the desired composition. Meanwhile, individual silicon and Sn films were deposited onto the new Cu foils using a 3-inch p-type silicon target (Kurt J. Lesker, 99.999% purity) and Sn target (Kurt J. Lesker, 99.998-99.999% purity) by pulsed DC magnetron sputtering for 20 and 40 min, respectively. All the films were subsequently stored under vacuum to prevent air exposure. 2032-type coin cells were assembled using the as-deposited films (1.6 cm^2) directly as the working electrodes, Li metal foil as the counter electrode, and 1.2 M LiPF$_6$ in ethylene carbonate (EC)-ethyl methyl carbonate (EMC) (3:7 by weight)
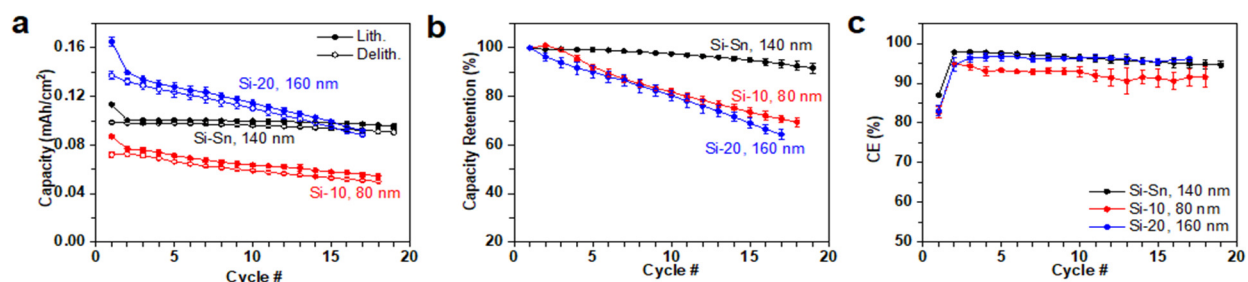
Figure 13 (a) Capacity, (b) capacity retention and (c) CE of Si-Sn and Si films of similar thickness.

as the electrolyte (Gen2). The cells were cycled between 1.5 and 0.01 V at C/20 based on the experimental capacity.

Figure 13 shows the cycling performance of the silicon and silicon-Sn films synthesized in FY18 Q4. Of note, both silicon and silicon-Sn films were deposited on Cu foils with roughened surface and films of a similar thickness are presented for a more direct comparison. As shown in Figure 13, silicon-Sn film exhibited much

better cycling stability than both silicon films of similar thickness with no obvious difference in coulombic efficiency (CE). These results clearly show the improved cycling performance of silicon-Sn compared to silicon. Further studies on understanding the superior cycling performance of silicon-Sn such as the phase evolution upon lithiation/delithiation and electrochemical/chemical stability of silicon-Sn vs. silicon will be pursued later.
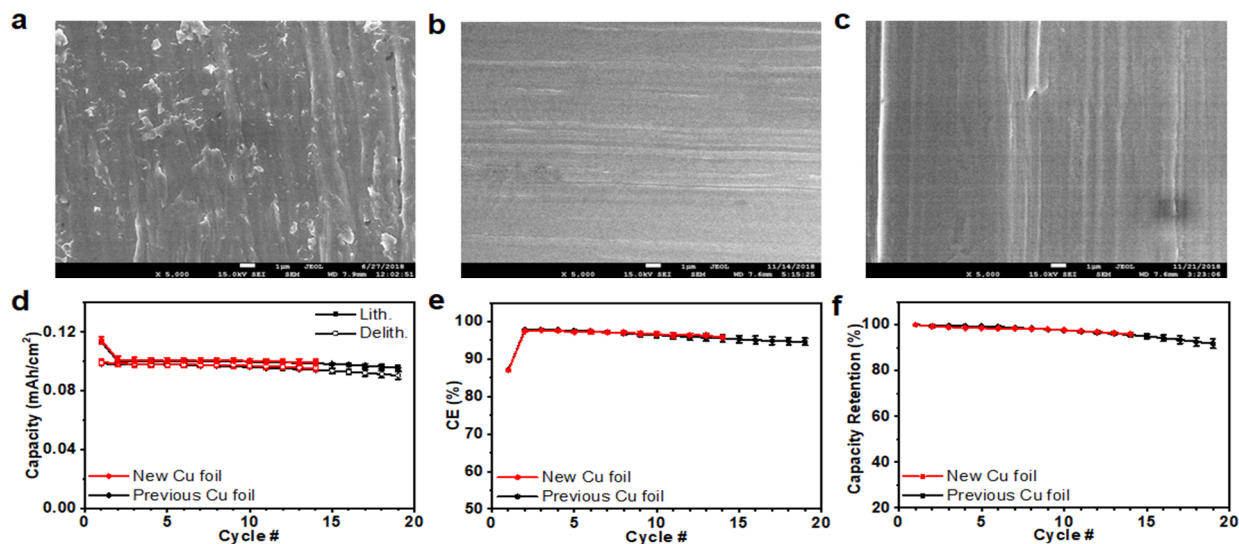
Figure 1 SEM images of (a) previous Cu foil, (b) new Cu foil and (c) Si-Sn film on new Cu foil, scale bar is 1 µm. Comparison of Si-Sn films on previous and new Cu foil: (d) lithiation/delithiation areal capacity, (e) CE and (f) capacity retention upon cycling.
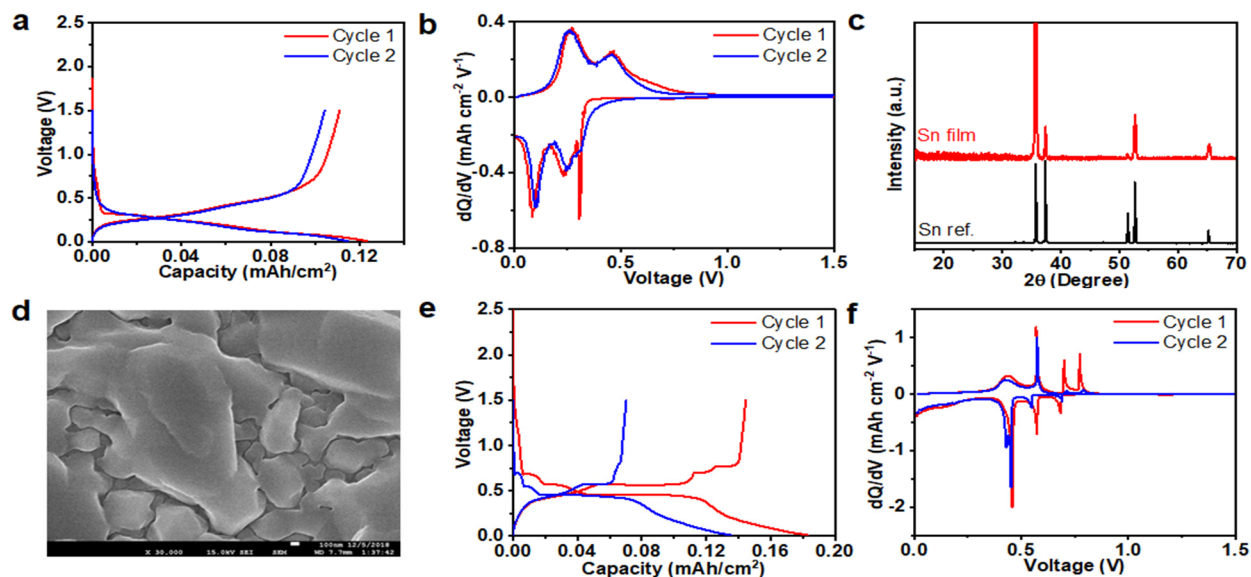
Figure 12 (a) Voltage profiles and (b) dQ/dV plots of Si film, (c) XRD, (d) SEM image, scale bar is 100 nm, (e) voltage profiles and (f) dQ/dV plots of Sn film.

Figure 14 displays the change in the Cu foil substrate. As shown in Figure 14a, b, the new Cu foil is featured by smooth surface with less roughness compared to the previous Cu foil. siliconngle silicon-Sn target was used to prepare the silicon-Sn film on the new Cu foil substrate at the identical sputtering condition to verify the effectiveness of the new Cu foil substrate. The as-produced silicon-Sn film on the new Cu foil (Figure 14c) resembles the morphological features of its Cu substrate. Figure 13d-f compares the cycling performance of the Si-Sn composite on previous Cu of roughened surface and new Cu of smooth surface, regarding lithiation/delithiation areal capacity, CE and capacity retention, respectively. The new silicon-Sn film exhibits comparable cycling performance, as evidenced by quite stable cycling capacity and small range bar, despite the differed surface roughness. Therefore, the new Cu foil was verified for the effective use as film substrate in the future thin film deposition. Indeed, silicon-Sn films demonstrates promising electrochemical performance and more robustness in film preparation. Synthesis of silicon-Sn thin splats will be conducted via splat quenching method. In order to further optimize the composition, thin films via co-sputtering multiple targets will be pursued, which will enable the feasibility to tune the compositions of varied stoichiometry and/or elements. The ultimate goal of this task is to produce silicon-based thin films as model electrodes for interfacial studies and provide guidance for the synthesis of silicon-based thin splats via splat quenching method. Thin films via co-sputtering of multiple targets requires the use of a new sputtering instrument. We first explored the deposition condition for individual silicon and Sn films for the co-sputtering of silicon-Sn films. Figure 14a, b present the voltage profiles and dQ/dV plots of the as-produced silicon film during the first two cycles. Of note, the new silicon film prepared by sputtering for 20 min is thinner, with a thickness of 146 nm, compared to the previous Si-20 (160 nm). It demonstrates typical lithiation of a-silicon, and formation of amorphous Li_xSi (a-Li_xSi) occurred around 0.25 V, whereas two broad peaks around 0.3 and 0.5 V appear during the delithiation process, corresponding to the Li extraction from a-Li_xSi. On the other hand, Sn tends to crystallize and agglomerate. As shown in Figure 14c, crystalline Sn reflections were obviously revealed by XRD, and the as-produced Sn film was composed of particles of a few hundred nanometer to 1 μm (Figure 14d). Upon lithiation/delithiation, voltage plateaus that are characteristic of crystalline Sn are clearly observed in Figure 14e, f. The initial CE of the as-produced Sn film was relatively low (78.89%) and it also displayed a fast capacity decay. This may be attributed to the thick Sn film (480 nm), further studies in Sn film deposition are underway to identify the optimal processing condition.

Conclusions

Si-Sn film deposited on new Cu foil substrate of smooth surface from single target showed identical electrochemical performance to that of the silicon-Sn film on previous Cu foil. Meanwhile, a-silicon and crystalline Sn films were deposited using a new sputtering instrument capable of co-sputtering from multiple targets, which enables the composition optimization of varied stoichiometry and elements. Based on the current studies on individual silicon, Sn and silicon-Sn, silicon-Sn films demonstrated much stable cycling performance and more robustness in film preparation compared to its individual component. Further studies on the interfacial properties of silicon-Sn films will be pursued. Meanwhile, co-sputtering of silicon and Sn will be explored on the new sputtering instrument in the next quarter for the compositional optimization.

High Silicon Content Anodes

Carbon-coated silicon for Improved Electrochemical Performance in Full Cells (ANL)

M.-T.F. Rodrigues, S.E. Trask, D.P. Abraham (Argonne National Laboratory)

Background

The use of blended silicon-graphite (silicon-Gr) negative electrodes increases the energy density of lithium-ion cells over those containing only graphite (Gr) electrodes. However, volume changes in the silicon particles that occur during cycling causes deterioration of the solid-electrolyte interphase (SEI) layer on the particles resulting in further electrolyte reduction that immobilizes Li$^+$ ions and, therefore, capacity fade. Various approaches are being actively pursued to improve the performance of silicon-based negative electrodes, which include using

- optimally sized silicon to prevent particle fracture and minimize reactions with the electrolyte,

- appropriate binders that allow electronic conduction while maintaining electrode integrity during cycling,

- electrolyte additives that enhance the stability of the silicon particle-electrolyte interface, which is continually disrupted during silicon expansion and contraction exposing fresh surfaces for solid electrolyte interphase (SEI) formation that trap additional lithium.

Another approach is to alter the silicon particle surfaces through use of coatings. Our previous work has shown that carbon coatings on silicon particles minimizes hydrogen generation during the preparation of electrode slurries. In addition, full cells containing the carbon-coated silicon particles display higher initial capacity, and greater capacity retention, than cells containing non-coated silicon particles.

We continue to examine the electrochemical performance of electrodes and cells containing these carbon-coated silicon particles (from Paraclete Energy). Here we report the long-term cycling performance of full cells with positive electrodes containing NCM523 (Li$_{1.03}$(Ni$_{0.5}$Co$_{0.2}$Mn$_{0.3}$)$_{0.97}$O$_2$) and negative electrodes (*not calendared*) containing the carbon-coated silicon. These negative electrodes were prepared at the CAMP facility and contained the following constituents:

- 15 wt% silicon, 73 wt% Graphite, 2 wt% C45, 10wt% LiPAA (henceforth referred to as 15Si)

- 70 wt% silicon, 15 wt% C45, 15 wt% LiPAA (henceforth referred to as 70Si)

Coin cells with the above electrodes, Celgard 2325 separator, and the Gen2 electrolyte with 10 wt% FEC were assembled in an Ar atmosphere glove box and tested on a Maccor cycler using standard cycling protocols.

Results

The discharge capacity vs. cycle number for the NCM523/15Si and the NCM523 cells, tested over 400 cycles at 30 °C, are shown in Figure 15. Henceforth all capacities are listed as mAh/g$_{oxide}$, wherein the oxide refers to the weight of the NCM523 component in the positive electrode. For the 15Si cell, the charge and discharge capacities during the 1st C/20 cycle are 179 and 136 mAh/g$_{oxide}$, yielding a coulombic efficiency (CE) of 76%; the corresponding values for the 70Si cell are 183 and 131 mAh/g$_{oxide}$, yielding a CE of 72%. The difference in values result from a greater loss of Li$^+$ ions to the SEI in the 70Si cell during the first charge cycle as the silicon expands during particle lithiation. The capacities continue to decrease during the early cycles indicating continued SEI formation; however, the CE increases with cycle number indicating progressively decreasing Li$^+$ loss to the SEI with cycling. For the 15Si cell, the charge and discharge capacities during the 3rd C/20 cycle are 135 and 134

mAh/g$_{oxide}$, yielding a CE of 99%; the corresponding values for the 70Si cell are 129 and 124 mAh/g$_{oxide}$, yielding a CE of 96%. That is, the values continue to be lower for the 70Si cell.

Below, Figure 15 shows that the biggest difference between the 15Si and 70Si cell arises at the onset of the C/3 cycling (cycle 4); the discharge capacities of the15Si and the 70Si cell are 128 and 108 mAh/g$_{oxide}$, indicating that fewer silicon particles are accessed when the 70Si electrode is cycled at the higher rate (C/3 vs. C/20). Participation of more silicon particles in the 70Si electrode could be improved by improvements in electrode design, which could include altering the contents of the conducting carbons/binder and through appropriate electrode calendaring.

Figure 15 indicates that the capacity differences between the 15Si and 70Si cells decreases with cycling. The 15Si cell loses capacity at a faster rate, especially during the 1st 100 cycles, compared to the 70Si cell. The faster capacity loss results from a greater volume changes in the silicon particles during lithiation/delithiation of the 15Si electrode. These greater volume changes continuously expose new surface area for SEI formation leading to a faster Li$^+$ loss. Thus at cycle 100 (C/20 rate), the charge and discharge capacities for the 15Si cell are 86 and 85 mAh/g$_{oxide}$, and the corresponding values for the 70Si cell are 84 and 83 mAh/g$_{oxide}$, respectively. After cycle 200, the plots for both cells overlap indicating that the capacity loss is determined by the amount of capacity transferred during the cycling, rather than the silicon content of the electrode. Perhaps, more interestingly, the cells contain cyclable Li$^+$ ions even after 400 cycles. In contrast, our previous studies with the 50-70 nm NanoAmor silicon (not coated) indicated negligible cyclable Li after only 200 cycles.
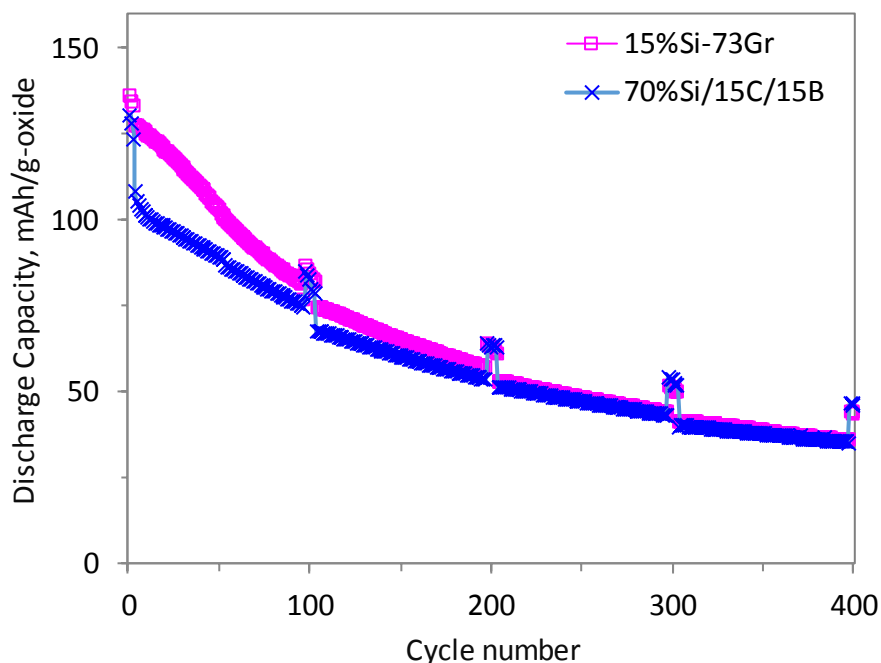
Figure 15. Discharge capacity vs. cycle number for an NCM523/15Si cell (magenta plot) and an NCM523/70Si cell (blue plot) tested at 30°C. The test protocol contained four repetitions of 100 cycles. In each of these 100 cycles, cycles 1-3 are at a ~C/20 rate, 4-97 are at a ~C/3 rate and 98-100 are at a C/20 rate.

Conclusions

We compared the long-term cycling behavior of NCM523/15Si and NCM523/70Si cells containing 150 nm carbon-coated silicon from Paraclete Energy. The highlights from our data are as follows:

- The initial capacity of the 15Si cell is slightly greater than that of the 70Si cell. The latter cell shows lower capacity when the cycling rate increases from C/20 to C/3 indicating that fewer silicon particles participate in the electrochemical reactions.

- The 15Si cell loses capacity much faster than the 70Si cell, especially during the first 100 cycles. This greater loss results from greater volume expansion of the silicon particles in the 15Si electrodes.

- Capacities of the 15Si and 70Si are similar after ~200 cycles indicating that fade rate is determined by the amount of charge transferred in the cell and not by the silicon content in the electrode.

- Both cells contained cyclable Li^+ ions even after 400 cycles, indicating that the carbon-coated silicon has better electrochemical performance than previously studied silicon. Nevertheless, significant performance improvements are needed to enable widespread use of these cell chemistries.

Carbon-Coated Silicon Materials

Gao Liu (LBNL)

Background

We are addressing the large volume change and excessive surface reactivity of silicon-based materials during lithiation and delithiation reactions by utilizing a carbon coating as an electronically conductive medium and electrolyte buffering layer to encapsulate the silicon particles. Despite the improved capacity retention of the silicon-based material by carbon coating, there have been fewer mechanistic investigations of silicon materials that incorporate a carbon coating. Variables include utilizing different carbon precursors for performing the carbon coating, which produce carbon coatings with different chemical and morphological carbon coatings. Here, we report the drastically different silicon solid state transformation during electrochemical process due to the different types of carbon precursors and carbon coatings on the same silicon nanoparticles.

High temperature thermal based carbonization process is used to produce carbon coating on silicon nanoparticles. Organic based precursors are used to form carbon coatings. Different precursors tend to form carbon coating with different morphologies. Two types of carbon coatings can be formed on silicon, (1) is a highly graphitized and dense coating derived from a polymer precursor (silicon/C-P), and (2) is disordered carbon structures derived from a sucrose precursor (silicon/C-S). The silicon materials with the graphitized coating deliver higher gravimetric capacity and stable cycling when compared to that of the silicon with disordered carbon coating. The large peak at 430 mV has been associated, using solid state Li NMR, with the conversion of a crystalline $Li_{3.75}Si$ to the amorphous silicon with a composition approximating $Li_{1.1}Si$ by Ogata et al., (Nature Comm, 2014). The enhanced cycling of the more graphitic coating appears to be associated with initial formation of the crystalline $Li_{3.75}Si$ endmember phase, however on cycling its re-formation is notably diminished. In contrast the silicon/C-S with an amorphous structure after 1st cycle, and does not clearly form the endmember phase during delithiation, as shown in Figure 16.
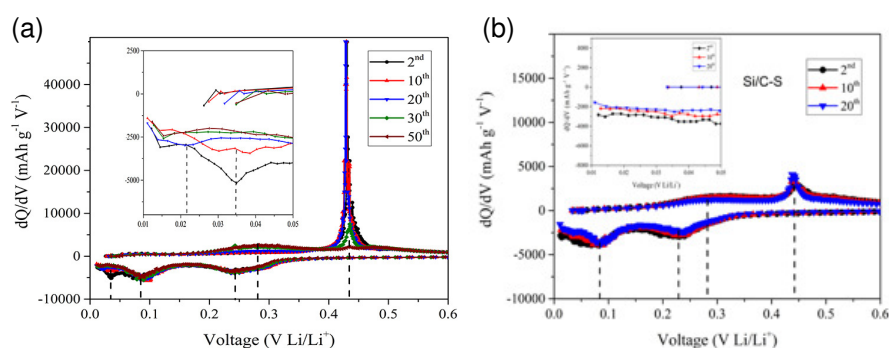
Figure 16. The dQ/dV plots of silicon/C composite electrodes show the phase transformation and crystallinity of the phases. (a) The silicon electrode with a highly graphitized and dense coating from a polymer precursor (silicon/C-P), the silicon/C-P materials maintains a two-phase reaction during the first 30 cycles (b) The silicon electrode with a sucrose precursor-based coating (silicon/C-S) has a carbon coating that is more disordered. The silicon/C-S forms an amorphous structure after 1st cycle.

High Silicon Content Electrodes: CAMP Prototyping

A.N. Jansen, S. Trask, B. Polzin, A. Dunlop, D. Kim, Joel Kirner, Wenquan Lu

Background

The CAMP Facility is continuing its focus on high-silicon (graphite-free) electrode formulations that it began in FY18. One key aspect of this work is too minimize the degree of silicon particle volume expansion and contraction by limiting the voltage window of the anode. Previous efforts utilized lithiation to as low as 10 to 50 mV versus Li+/Li, with limited success. Effort in this first quarter was focused on comparing the performance of electrodes designed with 50 mV and 100 mV lithiation cutoff potentials using three batches of silicon material from Paraclete Energy, including one of these Si batches that was roasted in air at 400°C. Two high-silicon content compositions were used:

71:10:19 wt.% (silicon : conductive additive : LiPAA binder)

80:10:10 wt.% (silicon : conductive additive : LiPAA binder)
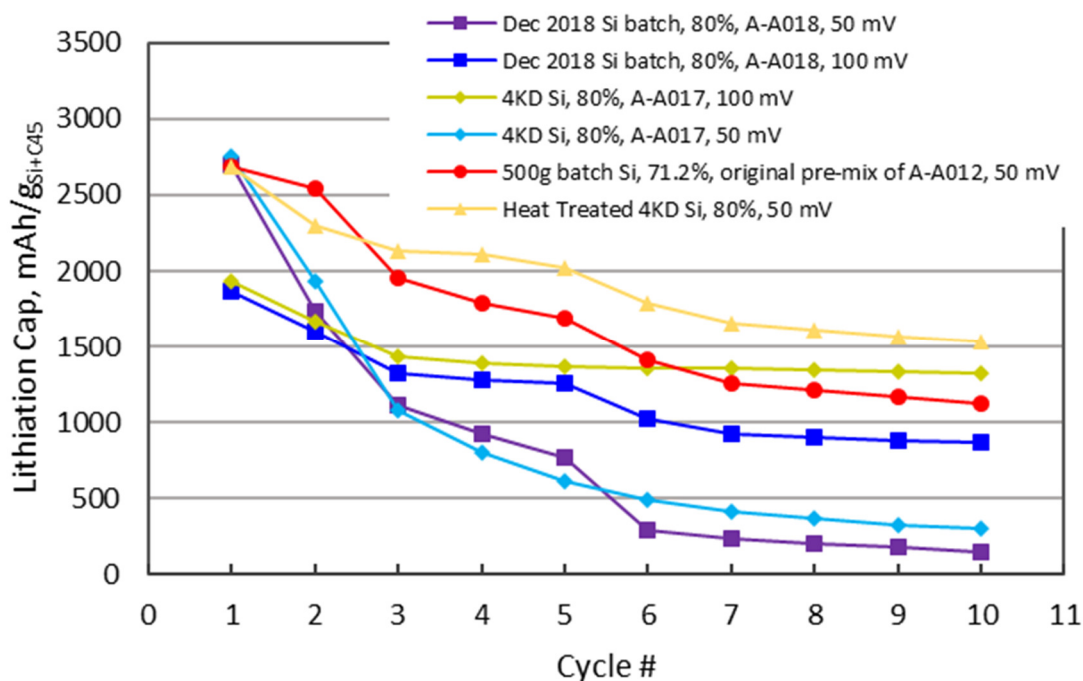
Figure 17. Lithiation capacity versus lithium metal for various graphite-free silicon electrodes fabricated by the CAMP Facility. These cells were cycled between 0.05 to 1.5 V or 0.1 to 1.5 V vs. Li+/Li as noted in the legend.

Results

The half-cell performance of these cells is shown in Figure 17. It is apparent from this plot that the capacity utilization and fade rate vary significantly between electrodes. But what is clear is that the first lithiation capacity is very consistent for the elctrode sets using a 50 mV cutoff potential and those using a 100 mV cutoff potential. Another observation is that the heat treatment in air at 400°C enhances the capacity utilization of

the silicon. Such improvements from heat treating were also seen with another source of silicon, and thus, should be explored further for this electrode system. More discussion will be included at the end of this section.

Figure 18 is a comparison of the full cell performance of both the 15 wt.% silicon-graphite and high-silicon graphite-free anodes versus the NMC532 cathode baseline. Only the Si electrodes that properly matched the NMC532 capacity loading were included in this full cell study, including the original Si (15 wt.%) from NanoAmor (50-70 nm). The most obvious observation from this comparison is the similar excessive capacity fade rate, regardless of the amount or source of silicon. The performance of the various sources of Si at 15 wt.% is exceptionally similar. Regarding the 80 wt. % Si electrodes, the best capacity retention was seen for the Paraclete Si (black line) that was heated treated in air at 400°C. While the same Si that was not heat treated resulted in a lower capacity, the capacity fade rate was similar to all the other Si electrodes.
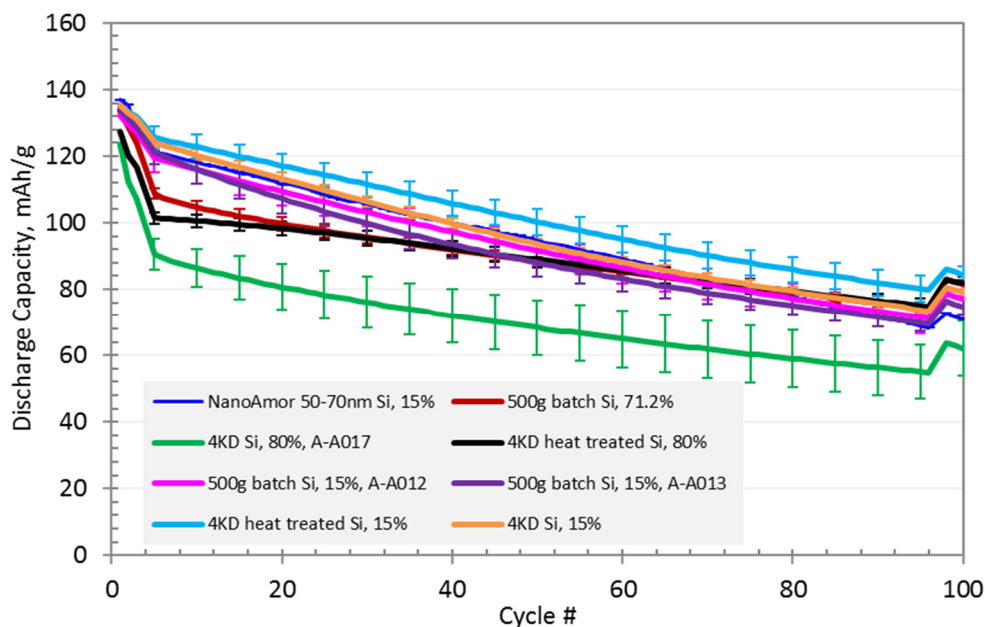
Figure 18. Full cell results using the silicon deep dive protocol for the high-silicon graphite-free anodes and 15 wt.% Si in graphite composite. All anodes were tested against a capacity-matched NMC532 cathode. The anode to cathode capacity pairing for the electrode couples was based on

Conclusions

Upon consideration of the half-cell and full-cell results, a portion of which was presented here, it is suspected that the difference in capacity utilization and fade rate for the high-silicon electrodes is most likely due to subtle uncontrolled variations in mixing and coating. These variations are magnified greatly due to the high capacity of silicon, which is ten times the capacity of graphite. It is also likely that the relatively lower concentration of conductive additive in these high-silicon electrodes creates situations were silicon particles can be more easily isolated from the electronic matrix of the electrode during cycling. Going forward, efforts will be directed to developing silicon electrodes with higher amounts of conductive additive – silicon content in the 50 – 70 wt.% range. It is also believed at this time that the heat treatment step improves the silicon contact to the binder and conductive additive used in the CAMP Facility's electrode fabrication process. Additional binder may be used to strengthen the physical properties of electrodes. Nonetheless, the silicon sources from Paraclete Energy remain a viable source of silicon to use as a baseline material.

Cell Balancing with High Silicon Content Electrodes

Baris Key, Binghong Han, Fulya Dogan, Jack Vaughey (ANL)

Background

A key attribute of a silicon electrode is the very high gravimetric capacity. This large capacity, while desirable, is associated with many other physical considerations that have hampered advancements in the field, notably high reactivity at high lithiation, volumetric growth, and uneven cation diffusion. As the effort moves to full silicon electrodes rather than silicon – graphite composites, issues associated with cell balancing and electrode thickness have arisen. Specifically cell balancing of these high capacity electrodes and identifying cathode
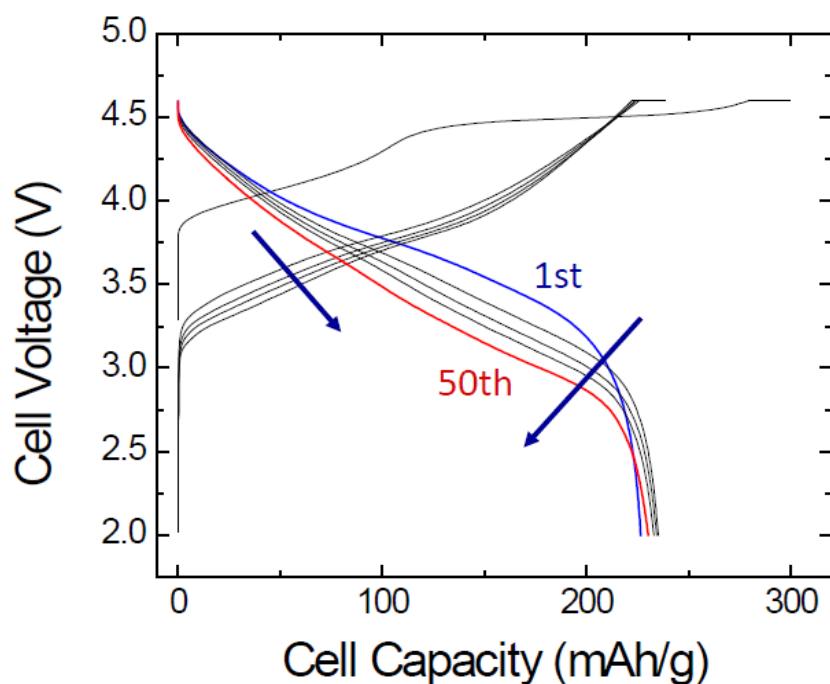
Figure 19. Capacity fade of the cathode sample associated with gradual defect consolidation and cation movement in the lattice.

electrodes that can be created to give acceptable n:p ratios to optimize cycling performance. The more common way to cell balance has been to use a very thin silicon electrode, however, issues associated with homogeneity (as seen in Rose Ruther's and Dan Abraham's electrode Raman spectroscopy studies), consistent thickness, and weighing errors are exasperated. In this quarter we worked with CAMP to optimize and evaluate a higher capacity cathode based on a commercial Li-rich NMC, $Li_{1.2}Ni_{0.25}Mn_{0.55}Co_{0.10}O_2$. These cathodes, capable of delivering 210-270 mAh/g (voltage window dependent), were assessed against a silicon anode of various capacities that allows for more accurate and dependable sample testing.

Results

Electrodes using Toda HE5050 (formula - $Li_{1.2}Ni_{0.25}Mn_{0.55}Co_{0.10}O_2$) were obtained from CAMP. The laminates were chosen for their high capacity and cycling mechanism that allows for lithium (formally as lithia) to be lost on the first cycle. This extra lithium was deemed an advantage as some of the lithium that comes off on the first cycle can be used as a compensatory source of lithium to offset the first cycle irreversibility of silicon that is associated
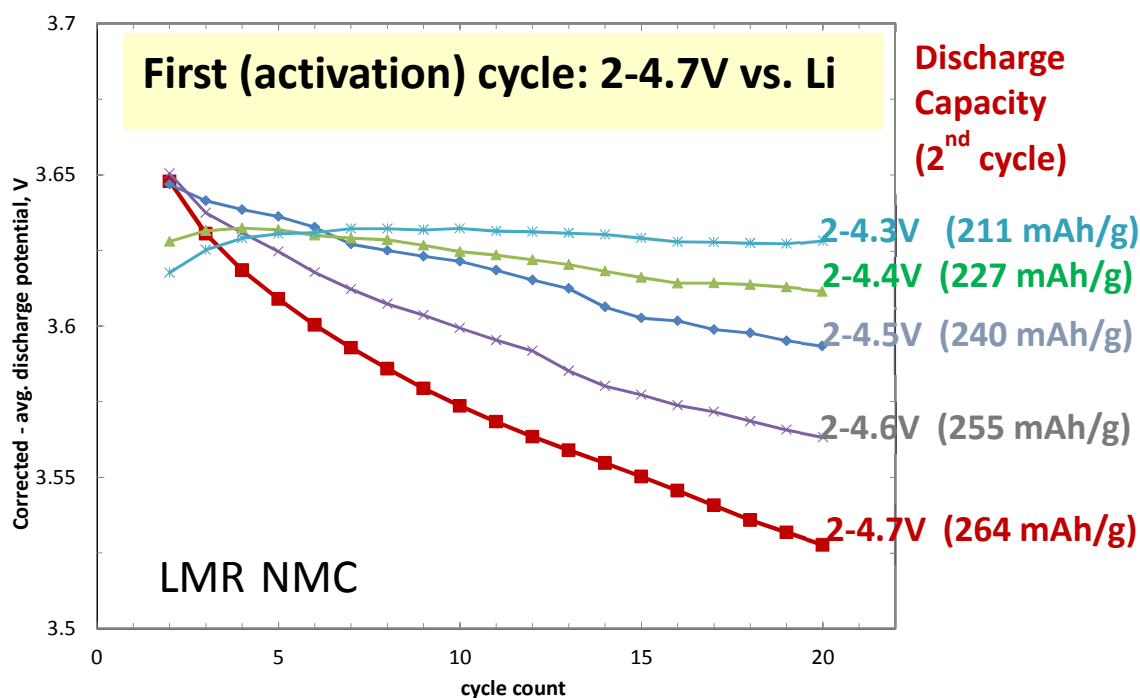
Figure 20. Capacity of LMR-NMC Cathodes as a function of upper cutoff voltage of $Li_{1.2}Ni_{0.25}Mn_{0.55}Co_{0.10}O_2$ while using a graphite anode.

with particle breakdown, SEI formation, and slow lithium diffusion into the bulk. This high capacity is achievable with electrochemical activation above 4.4V, the voltage at which defects and cations move and the O2p bands on the oxide anion start contributing to the observed capacity. This gradual re-arrangement of cations and defects results in 'voltage fade' as the electrode materials gradually 'relaxes' to a more stable state as seen in Figure 19.

In Figure 20, the utility of this extra available lithium is shown as a function of the upper cutoff voltage (graphite anode), with a jump in cell capacity at the cutoff voltage associated with the activation of the oxide sublattice. For a silicon-based cell, the 25% higher capacity of the LMR-NMC over the 532 NMC presently for the silicon/Gr composite anode cells may make it a better cathode baseline cell to evaluate higher silicon content electrodes. In Figure 21, we have evaluated an 80% silicon electrode (silicon811 CAMP) against an HE5050 LMR NMC cathode using a program standard Gen2/10FEC electrolyte. In a manner similar to the previous graphite study, the region before oxide activation is set at an upper cutoff voltage of 4.1V, while the expected

activation plateaus are evident in the 4.5V and 4.7V cutoffs. With regards to the Coulombic efficiency of the various cells, differences were noted especially for a formation cycle 4.7V cutoff (CE ~ 98.7%), while most of the other cells were CE ~ 99.2, slightly below the 532 NMC/Gr cell in the window 3-4.1V.
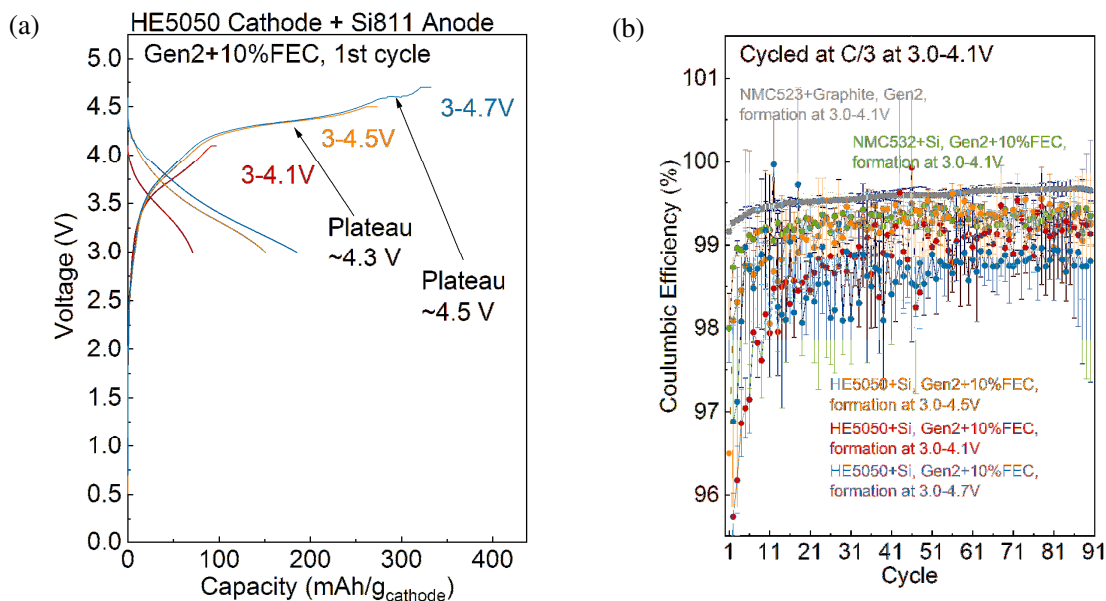
Figure 21. (a) Electrochemical evaluation of a silicon-rich electrode (silicon811) versus upper cutoff voltage for a HE5050 cathode. (b) Coulombic efficiencies of a silicon-rich electrode versus HE5050 using the window a 4.1 Upper Cutoff Voltage, but various windows (up to 4.7V) for formation cycling.

Conclusions

As the program moves to more silicon rich and high capacity anodes, higher capacity cathodes may be needed to maintain workable n:p ratios. The presently used NMC cathodes typically deliver ~180 mAh/g, while the HE5050 cathodes evaluated can deliver 220-260 mAh/g meaning the silicon electrodes used can have more typical thicknesses. Coulombic efficiencies for the cells were measured and consistent with previous studies. Structural and electrochemical characteristics of Li- and Mn- rich cathodes (HE5050) were found to be compatible with silicon electrodes and increasing the voltage cutoff during the formation cycles was an effective way to use the extra lithium to prelithiate the silicon and mitigate issues in silicon anode full cells.

Silicon Surface Functionalization

John Zhang, Sisi Jiang, Noah Johnson (ANL)

Background

In this quarter, surface functionalization of Si NPs was performed by a Pt catalyzed hydrosilylation reaction, i.e., organic functional groups were successfully attached to the surface of Si NPs via the insertion of C=C double bond to the silicon H bond. **Figure 22** shows the synthetic route of the first precursor 2 ((2 (allyloxy)ethoxy)methyl)oxirane (Allyl EO Epoxy) and the schematic of the synthesized Si NPs (silicon C3 EO Epoxy).
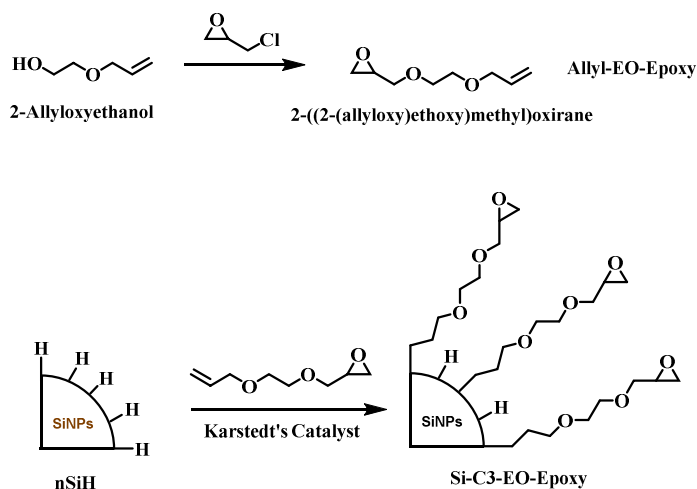
Figure 22. Synthesis of functional precursor containing an epoxy group and its hydrosilylation reaction with silicon-H terminated Si NPs.

The surface of the functionalized Si NPs was analyzed by ATR FTIR and compared with that of the pristine Si NPs (**Figure 23a**). The intensity of the silicon H stretching vibrational peak at 2100 cm^{-1} in the pristine particles is reduced after hydrosilylation reaction. In addition, part of the silicon H groups were converted its oxidized version OSi H (2250 cm^{-1}, higher wavenumber than silicon H) and silicon OH peak (3000 3500 cm^{-1}) showed up when the reaction was conducted in the open air. New peaks associated with the attached silicon C3 EO Epoxy functional groups appeared in the IR spectrum including the stretching vibration bands of C H at 2880 and 2930 cm^{-1}, C O at around 1050 cm^{-1}, silicon C at 1040 (overlapped with the C O bands) and epoxy ring breathing bands at 1250 1500 cm^{-1}, confirming the successful attachment of the epoxy containing functional groups onto the surface of Si NPs. Thermogravimetric analysis (TGA) showed a dramatic weight loss (26.2%) for the surface functionalized Si NPs made in glove box and reduced weight loss (13.3%) for the Si NPs made in the open air, while the pristine Si NPs only showed a negligible 0.4 % weight loss at 800°C (**Figure 23b**).
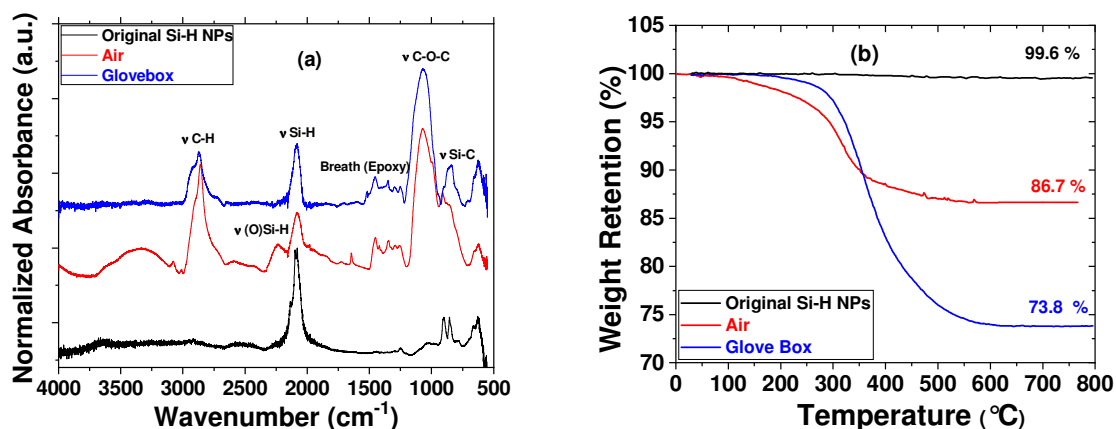
Figure 23. (a) FTIR spectra and (b) TGA thermograms of the epoxy-functionalized Si NPs. (*Black*: pristine Si NPs, *Red*: Si NPs synthesized in air, and *Blue*: Si NPs synthesized in Ar-filled glovebox).

The impact of the surface functionalization on the electrochemical performance was then investigated. Due to the limited amount of active material, silicon/graphite composite electrode with 15 wt.% Si NPs was fabricated and cycled using silicon-graphite/Li coin cells. The cells were subject to three formation cycles (C/20), followed by 150 cycles with a C/3 rate with a cutoff voltage of 0.01-1.5 V. The voltage profile for the first formation cycle is shown in **Figure 24a**, the first discharge (lithiation) and charge (delithiation) capacities of the pristine Si NPs, Si NPs synthesized in air and in the glovebox are 1013/695, 860/607, and 982/803 mAh/g, respectively, with the highest Coulombic efficiencies (82.3%) for the Si NPs with highest concentration of surface functionalities. The introduction of the functional group helps reduce the active lithium loss during the SEI formation process and the new surface acts as an artificial SEI stabilizing the electrode/electrolyte interface. **Figure 24b** showed the differential capacity (dQ/dV) profiles. Pristine electrode exhibited two obvious reduction peaks at ~ 1.3 V and 1.2 V, respectively, while the silicon-C3-EO-Epoxy electrodes showed only one (1.0 V for silicon-C3-EO-Epoxy-glovebox and 0.9 V for silicon-C3-EO-Epoxy-air) with relatively low intensities, indicating the SEI formation mechanism is quite different for the surface functionalized silicon anode.

The cycling performance of the cell was shown in Figure 25a. Silicon-graphite anode containing pristine Si NPs has an initial delithiation capacity of 552 mAh/g and it decreased in a few cycles before bounced back. The decreased capacity might be due to the electrolyte wetting issue. The initial capacity of the anode containing silicon-C3-EO-Epoxy is much higher (717 mAh/g) with a higher capacity retention (94.1%). However, for the anode containing silicon-C3-EO-Epoxy-air, the initial capacity increased (590 mAh/g) compared with that of the pristine, and the capacity retention is the highest (95.1%) among all studied materials.
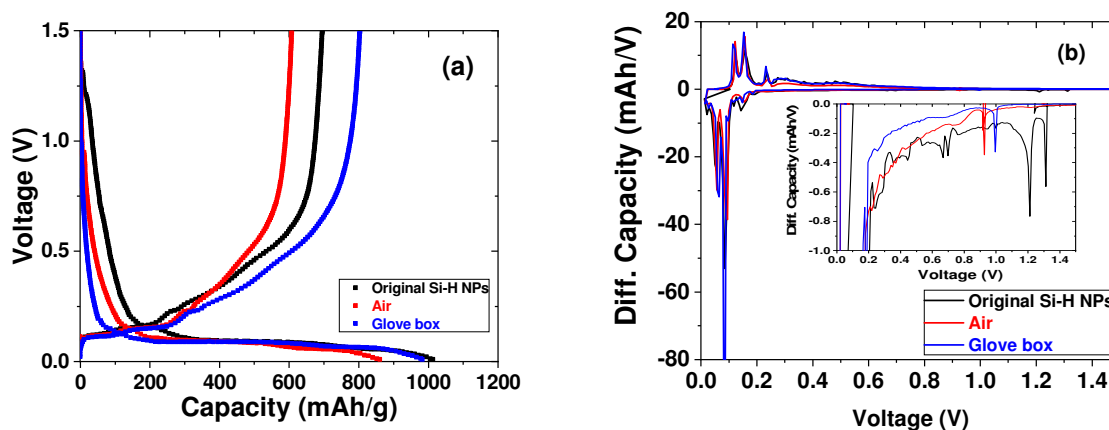
Figure 24. (a) The 1st formation cycle voltage profiles and (b) differential capacity profiles (dQ/dV) of electrodes based on pristine Si NPs, Si NPs synthesized in air and in glovebox (inset is an expansion of the dQ/dV plot during the lithiation process).

Anodes containing pristine Si NPs showed the first cycle Coulombic efficiency of 96.8%. In contrast, it increased to 98% for the Si NPs electrodes and stabilized at 99.7% (**Figure 25b**). This result clearly indicates the surface functional groups could sufficiently suppress the side reactions of the Si NPs preventing the active lithium loss at the anode/electrolyte interface.
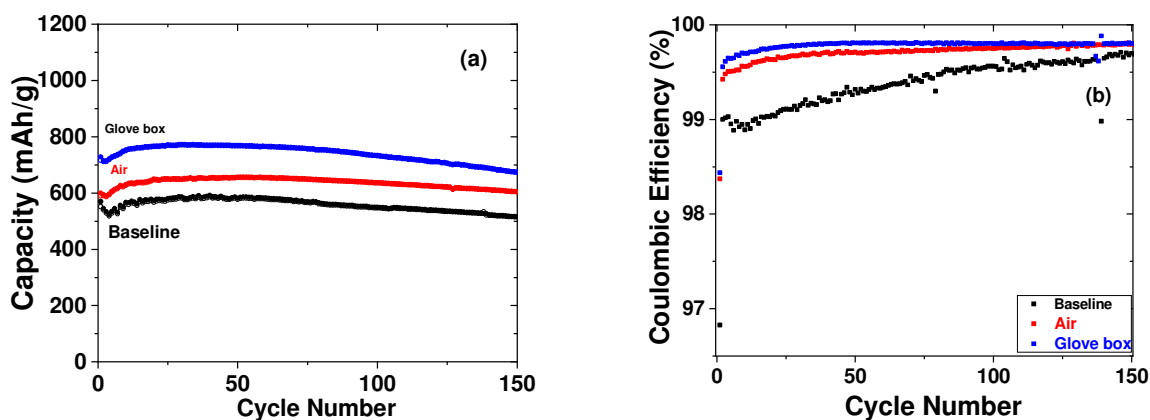
Figure 25. (a) Capacity retention (lithiation: solid; delithiation: empty) and (b) the Coulombic efficiency of silicon-graphite/Li cells.

Conclusions

We have successfully identified a second group of bi-functional electrolyte additives with methacrylate as reaction group and a hydrophobic or hydrophilic moiety as functional side groups. The dQ/dV tests are performed with this group of additives, showing systematic reduction of the voltage of reaction based on the bulkiness of the functional groups on the additives. This effect is more consistent with graphite electrode that that with silicon electrode. The hydrophobicity of the functional groups (i.e. dodecyl group) drastically reduce the lithiation voltage with silicon based electrode. The initial electrochemical characterizations are performed with lithium counter electrode cells. More systematic testing is being performed with full cells to fully characterize the additives' performance.

Lithium Inventory (Argonne National Laboratory)

Wesley Dose, James Blauwkamp, Ira Bloom, Maria Jose Piernas Muñoz, and Christopher Johnson (Argonne)

Background

For high energy density Li ion advanced cells that utilize silicon containing anodes, a concern of Li depletion and capacity fade during cycling is a real problem.   These silicon electrodes have large volume changes associated with (de)alloying reactions during cycling that causes the exposure of fresh silicon surfaces to the electrolyte. Further reactions take place to passivate these new surfaces, giving rise to a mechanism for ongoing depletion of the lithium inventory in every cycle.   In this project, we are developing tools to understand Li inventory and losses, where they may occur, and how. We also work on finding solutions to the capacity loss problem by up front loading cathodes with extra Li.

Results
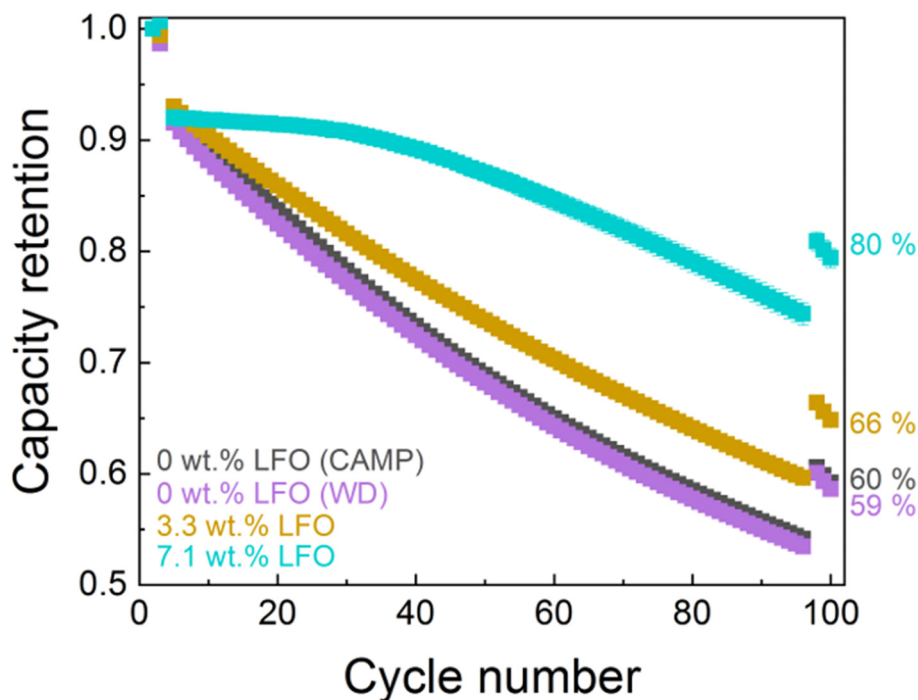
Figure 26. Normalized cathode capacity versus cycle number plot of two LFO weight percent blended NMC532 electrodes (as labeled) together with the non LFO containing silicon graphite full cells. In each case the silicon graphite electrode is from CAMP (A A013). Black markers show the baseline performance, where the NMC cathode is from CAMP (A C013B). The colored markers use a glove box cast electrode, with the magenta markers serving as a 0 % LFO proxy (baseline) for the LFO containing cells. Note the glove box cast electrodes (magenta (WD label)) match the performance of the CAMP full cells. The cyan curve shows 80% capacity retention after 100 cycles of C/3 cycling.

Lithium iron oxide (Li_5FeO_4 or LFO) has shown its effectiveness as a way of introducing lithium into a silicon containing cell to make it cycle with higher energy [1]. The release of 730 mAh/g capacity for LFO on the

initial charge cycle is key to introducing additional inventory of Li. LFO has addressed the problem of capacity degradation as was reported in silicon DD FY '18 final report. The capacity remains at 80% still after 100 cycles (Fig. 26).

In Figure 27, a plot of ASI versus OCP during HPPC tests indicates a much lower impedance to the LFO containing cell (Figure 27a). The hypothesis is that the state of charge (SOC) of the active cathode particles are lower when the Li inventory is increased within the silicon anode cell. Consumption of Li and ultimately SOC of the cell is buoyed by the extra Li inventory in the cell, which in turn, lowers the effective overcharge possibility that may occur with the NMC532 (3.0 to 4.1 V full cell) cathode particle. This hypothesis is supported by the SEM micrographs in Figure 27b or NMC532 particle cross sections that show the greater cracking in the NMC532 particle (top two micrographs) in the non LFO cell as compared to the type (bottom micrographs in Figure 27b) that has LFO blended with the NMC532 in the cell.

(a)   (b)
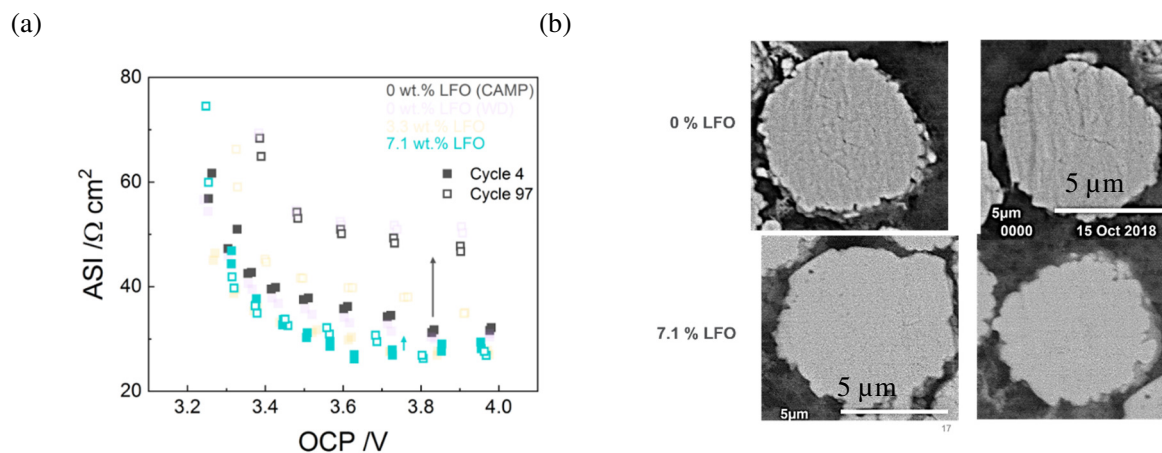
Figure 27. (a) Area specific impedance (ASI) of silicon graphite/LFO NMC532 full cells that shows lower impedance for the LFO containing cell (cyan markers) compared to the baseline (black markers) particularly after 97 cycles. Even after cycle 97, the ASI of LFO containing cell is still below 30 Ω cm^2. (b) FIB cross section SEM micrographs of the 0% LFO –NMC532 containing cell (100 cycles, above, top micrographs) showing cracks in the particle indicative of strain in the oxide (top), and the 7.1% LFO NMC532 containing cell (100 cycles, above, below micrographs) showing lack of cracks indicating crystal grain structural stability.

Conclusions

Some results of the LFO containing cells versus non LFO cells have been shown and discussed. We find that LFO containing NMC532 silicon full cells show better capacity retention and lower ASI than those cells devoid of blended LFO in them. Thus we predict that optimization of the amount of LFO in a silicon containing cell will be an important facet to study during cell tests (SLP) following larger coating attempts by CAMP facility to be undertaken in the next quarter.

References

[1] "Mitigating the initial capacity loss and improving the cycling stability of silicon monoxide using Li$_5$FeO$_4$", L. Zhang, W. M. Dose, A. D. Vu, C. S. Johnson, W. Lu, *J. Power Sources*, (2018), 400, 549-555.